

## **GRACEfully Closing the Water Balance**

### **A Data-Driven Probabilistic Approach Applied to River Basins in Iran**

Schoups, Gerrit; Nasser, M.

**DOI**

[10.1029/2020WR029071](https://doi.org/10.1029/2020WR029071)

**Publication date**

2021

**Document Version**

Final published version

**Published in**

Water Resources Research

**Citation (APA)**

Schoups, G., & Nasser, M. (2021). GRACEfully Closing the Water Balance: A Data-Driven Probabilistic Approach Applied to River Basins in Iran. *Water Resources Research*, 57(6), 1-27. Article e2020WR029071. <https://doi.org/10.1029/2020WR029071>

**Important note**

To cite this publication, please use the final published version (if applicable). Please check the document version above.

**Copyright**

Other than for strictly personal use, it is not permitted to download, forward or distribute the text or part of it, without the consent of the author(s) and/or copyright holder(s), unless the work is under an open content license such as Creative Commons.

**Takedown policy**

Please contact us and provide details if you believe this document breaches copyrights. We will remove access to the work immediately and investigate your claim.

# Water Resources Research



## RESEARCH ARTICLE

10.1029/2020WR029071

## GRACEfully Closing the Water Balance: A Data-Driven Probabilistic Approach Applied to River Basins in Iran

Gerrit Schoups<sup>1</sup>  and Mohsen Nasser<sup>2,3</sup> 

### Key Points:

- A Bayesian hierarchical model fuses water balance data containing unknown bias and random errors
- The model is solved using a combination of Markov Chain Monte Carlo sampling and iterative smoothing
- Computed posteriors provide hydrologically consistent data error and water balance estimates

### Supporting Information:

Supporting Information may be found in the online version of this article.

### Correspondence to:

G. Schoups,  
[g.h.w.schoups@tudelft.nl](mailto:g.h.w.schoups@tudelft.nl)

### Citation:

Schoups, G., & Nasser, M. (2021). GRACEfully closing the water balance: A data-driven probabilistic approach applied to river basins in Iran. *Water Resources Research*, 57, e2020WR029071. <https://doi.org/10.1029/2020WR029071>

Received 21 OCT 2020

Accepted 16 MAY 2021

<sup>1</sup>Department of Water Management, Faculty of Civil Engineering and Geosciences, Delft University of Technology, Delft, Netherlands, <sup>2</sup>School of Civil Engineering, College of Engineering, University of Tehran, Tehran, Iran, <sup>3</sup>Visiting Researcher, Department of Water Management, Faculty of Civil Engineering and Geosciences, Delft University of Technology, Delft, Netherlands

**Abstract** To fully benefit from remotely sensed observations of the terrestrial water cycle, bias and random errors in these data sets need to be quantified. This paper presents a Bayesian hierarchical model that fuses monthly water balance data and estimates the corresponding data errors and error-corrected water balance components (precipitation, evaporation, river discharge, and water storage). The model combines monthly basin-scale water balance constraints with probabilistic data error models for each water balance variable. Each data error model includes parameters that are in turn treated as unknown random variables to reflect uncertainty in the errors. Errors in precipitation and evaporation data are parameterized as a function of multiple data sources, while errors in GRACE storage observations are described by a noisy sine wave model with parameters controlling the phase, amplitude, and randomness of the sine wave. Error parameters and water balance variables are estimated using a combination of Markov Chain Monte Carlo sampling and iterative smoothing. Application to semiarid river basins in Iran yields (a) significant reductions in evaporation uncertainty during water-stressed summers, (b) basin-specific timing and amplitude corrections of the GRACE water storage dynamics, and (c) posterior water balance estimates with average standard errors of 4–12 mm/month for water storage, 3.5–7 mm/month for precipitation, 2–6 mm/month for evaporation, and 0–2 mm/month for river discharge. The approach is readily extended to other data sets and other (gauged) basins around the world, possibly using customized data error models. The resulting error-filtered and bias-corrected water balance estimates can be used to evaluate hydrological models.

## 1. Introduction

The increasing availability and accuracy of remote sensing data of the terrestrial water cycle holds great promise for calibration and validation of large-scale hydrological models. Several modeling studies have already taken advantage of these data for evaluating and constraining hydrological models, including water storage data from GRACE satellites (Bai et al., 2018; Scanlon, Zhang, Rateb, et al., 2019; Scanlon, Zhang, Save, et al., 2018; L. Zhang et al., 2017) and satellite-based evaporation data (Jiang et al., 2020; Lopez et al., 2017; Odusanya et al., 2019; Rientjes et al., 2013). A challenge with using remotely sensed data for model evaluation is that data errors need to be properly accounted for. Data errors are due to, for example, differences in scale, errors in the retrieval algorithms, and insensitivity of sensors to small changes in the variable being measured. However, without a reference “ground truth” data set, these errors are difficult to quantify, thereby undercutting the potential of remote sensing data for advancing large-scale hydrology. For example, ignoring or misrepresenting systematic data errors (bias) during calibration leads to biased parameter estimates and limits learning, especially when water balance data are hydrologically inconsistent, that is, they do not close the water balance. Furthermore, proper characterization of random errors (noise) and information content of the data is important: underestimating or even ignoring data noise may lead to overfitting, while overestimating data noise limits learning by not fully exploiting the information content of the data.

The processing and use of remotely sensed water balance data therefore requires (a) a methodology for estimating systematic and random errors in the data and (b) a methodology that corrects bias, filters out noise, and yields a hydrologically consistent set of water balance data that closes the water balance. These are of

© 2021. The Authors.

This is an open access article under the terms of the [Creative Commons Attribution](https://creativecommons.org/licenses/by/4.0/) License, which permits use, distribution and reproduction in any medium, provided the original work is properly cited.

course well-known challenges, and the following paragraphs review some of the approaches that have been proposed in the literature to tackle error estimation and correction of water balance data.

A common approach for estimating bias and random data errors of individual water balance variables is to compare the data to a reference ground truth data set (Moreira et al., 2019). For example, satellite-based precipitation estimates are often evaluated by using rain gauge data as ground truth (Beck et al., 2017; Massari & Maggioni, 2020), while errors in evaporation data products have been estimated by comparing to ground-based measurements from eddy covariance flux towers (M. Chen et al., 2016; Yang et al., 2017) and soil moisture sensors (Martens et al., 2017). Another approach to error estimation is to create a reference data set for the variable of interest by computing it as the residual of the water balance, with all other water balance components assumed to be known. This approach has mainly been used for evaporation (Liu et al., 2016; Wan et al., 2015; Weerasinghe et al., 2019). Regardless of the approach used for creating the reference data set, a conceptual drawback of the “ground truth” approach is that the “true” values are never actually measured, since no data set or estimate is completely error-free. For example, traditional ground observations, such as rain gauges, are limited in capturing variability across large areas, whereas remote sensing data suffer from uncertainties in converting electromagnetic signals into water balance variable estimates. Nevertheless, in practice, the ground truth approach may be justified as long as errors in the reference data set are sufficiently small relative to the data errors being estimated (Massari & Maggioni, 2020).

Alternative error estimation techniques that do not assume a reference ground truth data set have also been developed. The main idea is to use an ensemble of (three or more) data sets of the same water balance variable and either estimate errors based on variability across the ensemble (Tian & Peters-Lidard, 2010; Y. Zhang, Pan, Sheffield, et al., 2018) or based on a triple collocation or three-cornered hat method, as has been applied to precipitation (Alemohammad et al., 2015; Massari et al., 2017) and evaporation (Khan et al., 2018; Long et al., 2014) error estimation.

A separate group of studies focuses on bringing together estimates of the different water balance variables and modifying the original estimates so as to close the water balance (Aires, 2014; Allam et al., 2016; Hobeichi, Abramowitz, Contractor, & Evans, 2020; Munier et al., 2014; Pan, Sahoo, et al., 2012; Pan & Wood, 2006; Pellet et al., 2019; Rodell et al., 2015; Sahoo et al., 2011; Simons et al., 2016; Wang et al., 2015; Y. Zhang, Pan, Sheffield, et al., 2018; Y. Zhang, Pan, & Wood, 2016). In closing the water balance, variables with large errors are adjusted more than variables with small errors, a process that can be formalized by what Pan and Wood (2006) called a constrained Kalman filter. A crucial input for these water balance fusion studies is therefore the specification of the magnitude of errors in each water balance variable. In existing water balance fusion studies, error estimates are typically fixed a priori based on expert judgment or on results from the error estimation techniques mentioned in the previous paragraphs. However, combining error estimates from different studies for water balance closure easily leads to inconsistencies, for example, when error estimates of the different variables are based on conflicting underlying ground truth assumptions or on data from different regions. Furthermore, by fixing the data errors in advance, existing water balance fusion studies forego the opportunity to improve data error estimates: as we show in this paper, the idea of estimating errors by bringing together multisource data, as used in triple collocation for a single variable, can also be applied to water balance fusion where data on the different water balance variables are combined.

The current paper builds on previous efforts and combines the error estimation and water balance fusion steps into a single methodology that removes the need for a reference ground truth data set. Instead, each water balance variable is assumed to be subject to unknown bias and random errors, and a single iterative approach is used to estimate an internally consistent set of data errors and water balance variables that close the water balance. The methodology relies on the formulation of a probabilistic model that combines monthly basin-scale water balance constraints with data error models for each water balance variable. The data error models relate the observations to the underlying unknown true values and contain the unknown parameters to account for uncertainty in the data errors. The overall probabilistic model takes the form of a Bayesian hierarchical model with two levels of uncertainty: unknown water balance variables are constrained by probability distributions with parameters that themselves are treated as unknown random variables with specified prior distributions. After conditioning on available water balance data, posteriors of all unknowns, that is, error parameters and water balance variables, are computed using a combination of

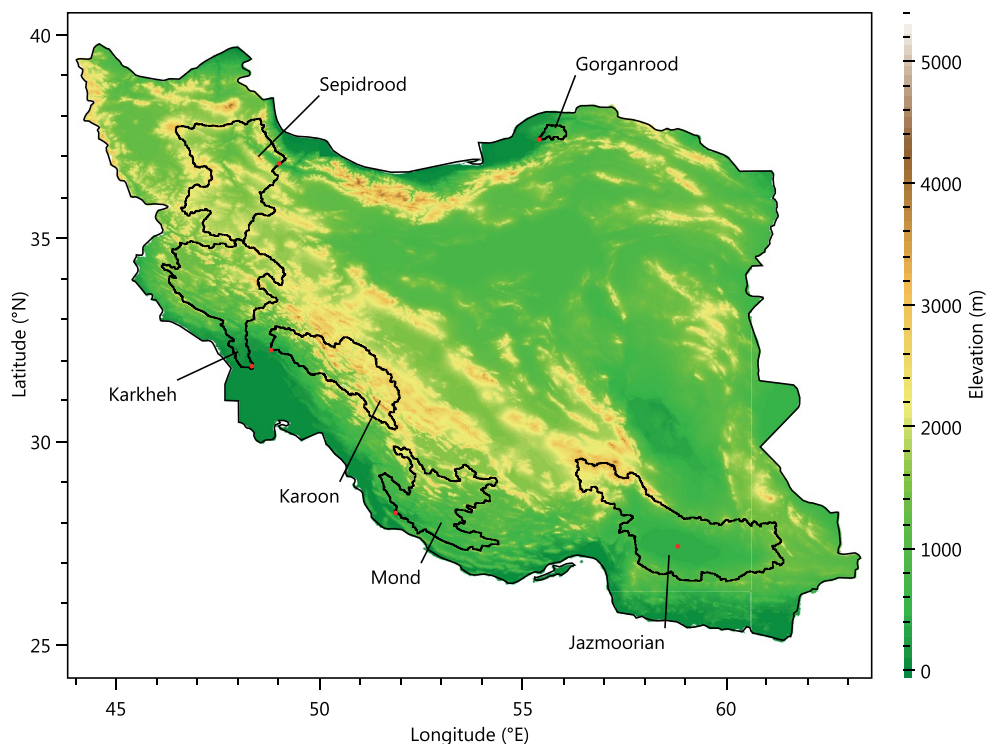


**Figure 1.** Topographic map of Iran with location of river basins and their outlets (red dots). The Jazmoorian basin is endorheic and drains to an internal lake.

Markov Chain Monte Carlo (MCMC) sampling and an iterative form of (Kalman) smoothing. The posteriors automatically fuse all available information and yield the best estimates with uncertainty for all water balance variables and error parameters. We note that (Kalman) smoothing, that is, estimating water balance variables using data from the entire time series, has not been used in previous water balance fusion studies, which have sometimes used additional postprocessing steps to remove high-frequency artifacts in the estimates (Munier et al., 2014).

The paper starts by introducing the river basins used in this study. Water balance data for these basins are used to motivate the development of the probabilistic data error models in Section 3. Section 4 details how the probabilistic water balance model is solved, that is, how the posteriors of interest are computed. Section 5 then presents the results of applying the methodology to river basins in Iran, followed by an evaluation of different assumptions in the analysis (Section 6) and a summary of the main findings.

## 2. Case Study: River Basins in Iran

Figure 1 shows the locations of the Iranian river basins investigated in this study. The basins were selected for their availability of river discharge data, their relatively large size, and their geographical location across the country from west to east. Basin boundaries were identified by delineating the topographically upstream areas for each stream gauge providing river discharge data (Table 1). The endorheic Jazmoorian basin drains to an internal lake without natural outlet and hence does not have a stream gauge recording outflow. The basins range in size from 1,600 to 70,000 km<sup>2</sup> and are generally semiarid or arid with potential evaporation equal to 1.4 to 5 times the average precipitation. Consequently, runoff ratios ( $Q/P$  in Table 1) are small, mostly 0.1 or less, with the exception of the relatively steep mountainous Karoon basin. Surface and groundwater withdrawals for irrigation are common and tend to further reduce runoff ratios. All basins have pronounced seasonality in precipitation and runoff, with relatively wet winters and dry summers, translating into seasonal wetting and drying cycles.

**Table 1**  
*River Basin Characteristics*

ID	Basin	Stream gauge (°N, °E)	Area (km <sup>2</sup> )	Elevation (m)	$\frac{E_p^*}{P}$	$\frac{Q^*}{P}$
1	Sepidrood	Gilvan (36.83, 49.02)	49,246	332–3,478	1.78	0.06
2	Karkheh	Abdolkhan (31.83, 48.36)	45,497	36–3,528	1.61	0.11
3	Karoon	Karoon-IV (32.25, 48.83)	32,840	66–4,199	1.36	0.38
4	Mond	Ghantareh (28.25, 51.87)	35,397	68–3,105	2.54	0.04
5	Jazmoorian	(Endorheic)	70,102	365–4,226	5.04	0.00
6	Gorganrood	Bustan Dam (37.42, 55.41)	1,620	85–1,994	2.04	0.06

Note. \* $P$ ,  $Q$ , and  $E_p$  are average precipitation, river discharge, and potential evaporation.

The generally water-stressed nature and complex topography of the selected river basins, coupled with significant interventions in the natural water cycle in the form of dams, irrigation, and groundwater pumping, provide a good test bed for the proposed water balance methodology.

### 3. Probabilistic Water Balance Model

Our interest is in estimating all the terms in the monthly basin-scale water balance:

$$S_t = S_{t-1} + P_t - E_t - Q_t \quad (1)$$

where  $S_{t-1}$  and  $S_t$  are the total water storage (surface and subsurface) in the basin at the start and end of month  $t$ ,  $P_t$ , and  $E_t$  are the basin average precipitation and evaporation (including transpiration), and  $Q_t$  is the river discharge at the basin outlet for month  $t$ . Each term is normalized by the basin area and expressed in consistent water depth units (e.g., mm). Equation 1 assumes the negligible net lateral groundwater flow into or out of the basin. It also assumes that no significant surface water flows crossing the basin boundary, except for the river discharge at the basin outlet. Thus, upstream inflows and inter-basin water transfers are considered negligible, while intra-basin water transfers, for example, via water diversions and groundwater pumping for irrigation, are captured by Equation 1. Inter-basin water transfer is known to occur from the upstream part of Karoon basin (Figure 1) into the semiarid Zayanderood basin to the north; the transferred amount of water is however negligible compared to the total runoff in Karoon basin (Abrishamchi & Tajrishy, 2005).

In principle, each term in Equation 1 can be measured or estimated independently. However, bringing such independent estimates together does not typically lead to water balance closure because all measurements and estimates are subject to systematic and random errors. Conceptually, it is then useful to distinguish between “true” and “observed” versions of each water balance variable: by definition, the true water balance variables close the water balance, and the true and observed versions of each water balance variable are related via data error models that capture systematic and random deviations between observed and underlying true values.

Each data error model consists of parametric probabilistic relations between observed and true values, where parameters quantify the magnitude of systematic and random data errors. Since the magnitude of these errors is not known a priori, the parameters are themselves treated as random variables with specified prior distributions. The resulting model can hence be viewed as a Bayesian hierarchical model with two levels of uncertainty, that is, one for error parameters and the other for water balance variables.

The monthly water balance data used here are summarized in Table 2. We follow previous water balance fusion studies and focus as much as possible on observational data instead of hydrological model outputs as the source for the water balance data, thereby minimizing the impact of hydrological process assumptions. An exception is the GLEAM evaporation product, which internally relies on a soil water balance model. All data were spatially averaged across each basin to obtain monthly basin-scale data values. The following

Variable	Symbol	Data source	Resolution	Reference
Precipitation	$P_{obs1}$	GPM IMERG Final V06B	0.1°	Huffman et al. (2019)
	$P_{obs2}$	CHIRPS v2.0	0.05°	Funk et al. (2014)
Evaporation	$E_{obs1}$	SSEBop v4	0.01°	Senay et al. (2020)
	$E_{obs2}$	GLEAM v3.3b	0.25°	Martens et al. (2017)
River discharge	$Q_{obs}$	Stream gauges	Basin	IWRMC (2020)
Storage	$S_{obs}$	GRACE JPL mascon RL06v02	3°	Wiese, Yuan, et al. (2018)

sections describe data sources and probabilistic data error models for each water balance variable ( $P$ ,  $E$ ,  $Q$ , and  $S$ ).

### 3.1. Precipitation Error Model

The first data set used is GPM IMERG (Table 2), which provides monthly precipitation values and associated standard errors. The monthly IMERG precipitation merges satellite-based estimates with the GPCC rain gauge data set, while standard error estimates are based on the methodology of Huffman (1997). There is generally a good correspondence between IMERG and spatially interpolated rain gauge precipitation for the basins studied here (Figures 2, S1 and S2), with the exception of Gorganrood basin. A recent evaluation of IMERG across Iran (Maghsood et al., 2020) reported small but systematic overestimation of the monthly precipitation in dry regions and underestimation in the wettest parts of the country. To account for potential bias in IMERG, we included CHIRPS as a second precipitation data set. In the semiarid Mond basin for example (Figure 2), CHIRPS tends to give lower precipitation than IMERG during the wet winter months.

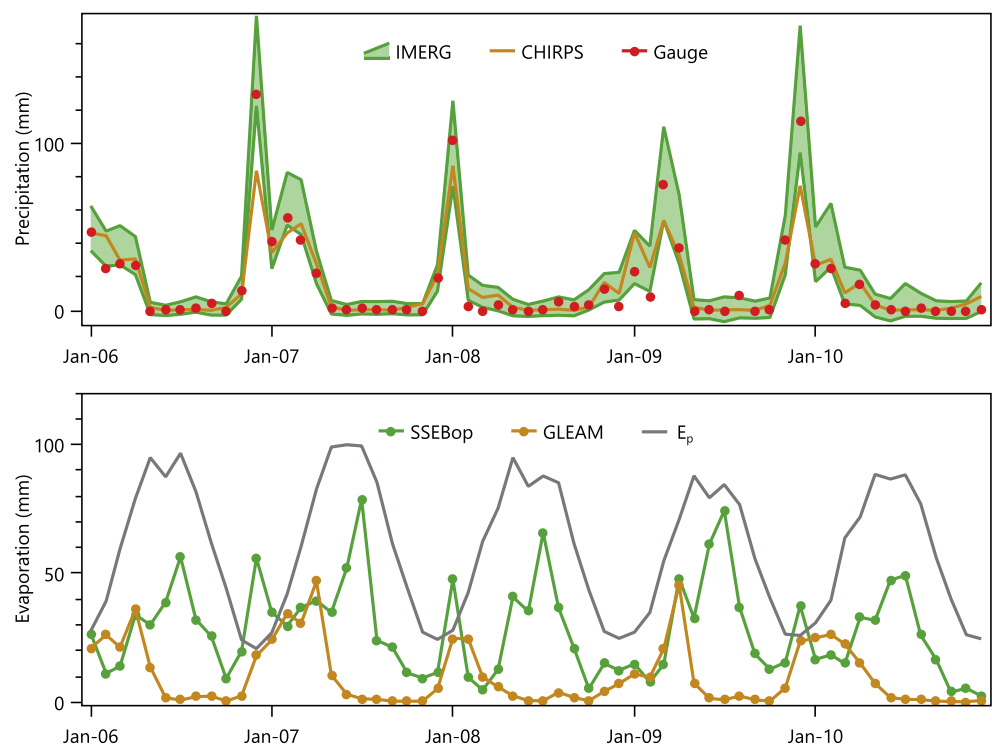


**Figure 2.** Monthly precipitation and evaporation data for Mond basin during 2006–2010. The IMERG data include standard errors and are plotted as 90% uncertainty bands. Spatially interpolated basin average rain gauge precipitation is included for comparison but was not used in the model. Potential evaporation from the GLEAM data set is shown as  $E_p$ .

The following error model was then used to relate the observed and true precipitation:

$$m_{P,t} = (1 - w_P)P_{obs1,t} + w_P P_{obs2,t} \quad (2)$$

$$s_{P,t} = \max\left(\sigma_{P,t}, \frac{1}{2}r_P |P_{obs1,t} - P_{obs2,t}|\right) \quad (3)$$

$$P_t \sim \mathcal{N}(m_{P,t}, s_{P,t}^2) \quad (4)$$

$$P_t \geq 0 \quad (5)$$

The first equation models bias in the observations by describing the prior mean precipitation  $m_{P,t}$  for month  $t$  as a weighted average of IMERG ( $P_{obs1,t}$ ) and CHIRPS ( $P_{obs2,t}$ ) monthly basin precipitation. Parameter  $w_P$  represents the weight; since it is unknown a priori, it is given a quasi-uniform prior between 0 and 1 (specifically, a logit-normal prior with location parameter  $\mu = 0$  and scale parameter  $\sigma = 1.4$ ) to reflect prior uncertainty about the bias.

The second equation models random errors in the observations by describing the prior standard deviation  $s_{P,t}$  of precipitation for month  $t$  as the largest of either (a) the IMERG standard error  $\sigma_{P,t}$  or (b) the scaled absolute difference between the two precipitation data sets for each month, using  $r_P$  as the scaling parameter. The reasoning behind this is that large differences between the two data sets may not only indicate systematic but also significant random errors. Parameter  $r_P$  is given a quasi-uniform prior between 0 and 1 to reflect prior uncertainty about the relation between bias and random errors. In the limit when  $r_P = 1$ , the prior standard deviation is half the absolute difference between the two data sets. However, to avoid unrealistically small prior uncertainty in precipitation, for example, when  $r_P$  is near 0 or the two data sets are in close agreement, the value of  $s_{P,t}$  is not allowed to be less than the IMERG standard error  $\sigma_{P,t}$ . The latter is obtained by arithmetic averaging of the gridded “random error” variable in the IMERG data set. This implicitly assumes that the IMERG random errors are spatially perfectly correlated across the basin. As such, it provides a conservative estimate of the magnitude of basin-scale random errors, since averaging partially uncorrelated grid-scale random errors would result in some error cancellation and therefore smaller values for  $\sigma_{P,t}$  at the basin-scale.

Finally, the last two equations in the precipitation error model treat the true precipitation  $P_t$  for month  $t$  as a random draw from a truncated normal distribution. Truncation at zero constrains precipitation to be nonnegative. Validity of the proposed precipitation error model will be evaluated a posteriori. Note that an alternative precipitation error model could treat the two data sets as independent random samples of the underlying true values. The proposed model does not assume such independence but instead, models random errors as deviations from the weighted average of the two data sets.

### 3.2. Evaporation Error Model

To capture the uncertainty and errors in evaporation, two different remote sensing evaporation products are used, that is, GLEAM and SSEBop (Table 2). These data sets use different methods for estimating the evaporation from remote sensing data. GLEAM uses Priestley-Taylor for potential evaporation and estimates the actual evaporation as a function of the microwave vegetation optical depth and soil moisture, in combination with a root-zone water balance. On the other hand, SSEBop uses Penman-Monteith for the potential evaporation and estimates the actual evaporation based on a surface energy balance and remotely sensed land surface temperature. For the basins studied in this paper, these two approaches translate into similar evaporation estimates under energy-limited conditions (wet winters) but significantly different evaporation estimates under water-limited conditions (dry summers). Figure 2 illustrates this for the Mond basin, with similar patterns observed in other basins (see Supporting Information): in the absence of significant rainfall during summer, GLEAM evaporation decreases to near-zero values, while SSEBop evaporation shows a peak in summer, suggesting that water remains available to natural vegetation or crops (irrigation). These differences result in significant prior uncertainty in evaporation during summers.

An error model similar to that of precipitation is adopted for evaporation:

$$m_{E,t} = f_E \left[ (1 - w_E) E_{obs1,t} + w_E E_{obs2,t} \right] \quad (6)$$

$$s_{E,t} = \max \left( 0.1 m_{E,t}, \frac{1}{2} r_E |E_{obs1,t} - E_{obs2,t}| \right) \quad (7)$$

$$E_t \sim \mathcal{N}(m_{E,t}, s_{E,t}^2) \quad (8)$$

$$E_t \geq 0 \quad (9)$$

Bias is modeled with two time-invariant parameters:  $w_E$  is a weight that interpolates between SSEBop  $E_{obs1,t}$  and GLEAM  $E_{obs2,t}$  evaporation, and  $f_E$  is an additional scaling factor that provides an additional degree of freedom to, for example, account for bias outside the range of the two data sets. Random errors are modeled using the same approach used for precipitation, with parameter  $r_E$  controlling to what extent prior uncertainty scales with the absolute difference between the two evaporation data sets. If the difference between the two data sets is small, for example, during energy-limited conditions in winter, a minimum relative error of 10% is assumed by setting  $s_{E,t} = 0.1 m_{E,t}$ . As with precipitation, true evaporation  $E_t$  in month  $t$  is treated as a random draw from a truncated normal distribution. Truncation at zero constrains evaporation to be nonnegative.

Since the values of the error parameters are not known a priori, they are given vague prior distributions: quasi-uniform priors between 0 and 1 for  $w_E$  and  $r_E$  (specifically, flat logit-normal priors between 0 and 1 with location parameter  $\mu = 0$  and scale parameter  $\sigma = 1.4$ ) and a lognormal prior for  $f_E$ , with mode at 1 (no bias) and a coefficient of variation CV of 50%.

### 3.3. River Discharge Error Model

We assume that the basin is gauged and a possibly incomplete record of measured monthly river discharge data  $Q_{obs}$  is available. A proportional error model is used to relate these data to the underlying true discharge values  $Q$ :

$$m_{Q,t} = \mathcal{N}(Q_{obs,t}, v_{Q_{obs,t}}) \quad (10)$$

$$s_{Q,t} = a_Q Q_{obs,t} + b_Q \quad (11)$$

$$Q_t \sim \mathcal{N}(m_{Q,t}, s_{Q,t}^2) \quad (12)$$

$$Q_t \geq 0 \quad (13)$$

For months with observations, we set  $v_{Q_{obs,t}} = 0$  so that the first equation becomes equivalent to  $m_{Q,t} = Q_{obs,t}$  that is, the mean of  $Q_t$  is equal to the (unbiased) observation for that month. For months with missing observations,  $Q_{obs,t}$  and  $v_{Q_{obs,t}}$  are set equal to the mean and variance of the river discharge observed for that month across the entire observation record. This procedure works as long as only a few observations are missing. For the basins studied in this paper, Gorganrood basin has 1 month with missing data and Mond basin has 3 months with missing observations.

The magnitude of random observation errors is controlled by the standard deviation  $s_{Q,t}$ , which is modeled as a linear function of the observed discharge for that month (or, the mean historical discharge for that month in case of a missing observation). This model assumes that observation errors increase linearly with discharge and include two time-invariant parameters,  $a_Q$  and  $b_Q$ . Parameter  $a_Q$  is given a log-normal prior with mode at 0.1 (i.e., a relative error of 10%) and a small CV of 1%, while  $b_Q$  is given a log-normal prior with mode at 0.001 and also a CV of 1%. Hence,  $a_Q$  and  $b_Q$  are more or less kept fixed a priori. The sensitivity of the results to the assumed narrow prior of  $a_Q$  will be evaluated in Section 6.

As with precipitation and evaporation, the monthly discharge  $Q_t$  is constrained to be nonnegative.

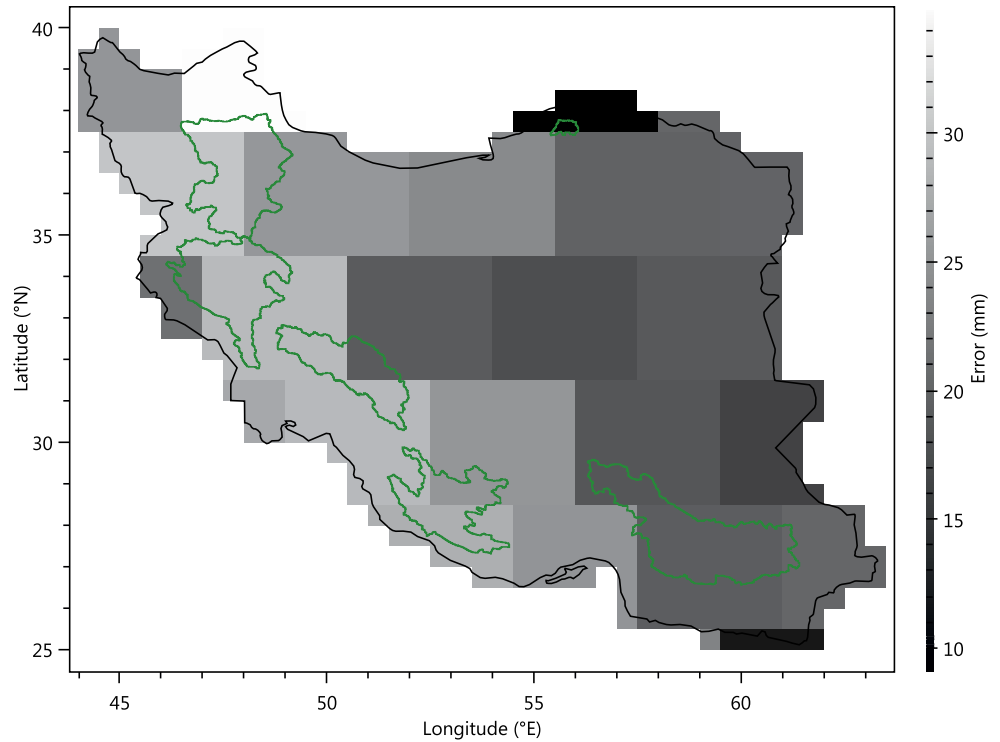


**Figure 3.** Time-averaged (2006–2015) measurement errors of the JPL GRACE data for each 3° mascon across Iran (based on the “uncertainty” variable in the JPL netCDF data set). Errors tend to be smaller in arid parts of the country (east and central).

### 3.4. Water Storage Error Model

The JPL mascon GRACE water storage data used here (see Table 2) consist of monthly total terrestrial water storage anomalies relative to the period 2004–2009 at a spatial resolution of 3°. The data come post-processed with the Coastline Resolution Improvement (CRI) filter by Wiese, Landerer, and Watkins (2016) to reduce leakage errors across land-ocean boundaries. Figure 3 shows measurement errors of the GRACE data across Iran.

Wiese, Landerer, and Watkins (2016) used simulations with the Community Land Model to downscale the coarse 3° storage data to a 0.5° global grid. Here, we use an alternative approach and instead downscale the data directly to the river basin of interest without using a hydrological model: first, the 3° data are weighted area averaged over each river basin, and then an error model is specified to quantify systematic and random differences between the basin-averaged storage data and the true storage changes in the basin.

Both the monthly basin-scale data and the true storages typically have a seasonal cycle, but with possibly different amplitudes and phases because the coarse-scale data are polluted by storage dynamics outside of the basin (“leakage”). This motivates the following noisy sine wave error model for quantifying the differences between GRACE basin-scale water storages  $S_{obs,t}$  and underlying true storages  $S_t$ :

$$m_{S,t} = S_t + A \sin\left(\omega\left(\frac{t}{12} - \delta\right)\right) \quad (14)$$

$$s_{S,t} = \sigma_S \quad (15)$$

$$S_{obs,t} \sim \mathcal{N}(m_{S,t}, s_{S,t}^2) \quad (16)$$

Here,  $A$  is amplitude (mm),  $\omega$  is the frequency (radians per year), and  $\delta$  is the phase (in years) of the errors. This model accounts for systematic differences in amplitude and phase between the observed and true values by means of time-invariant error parameters,  $A$  and  $\delta$ . Furthermore, time-invariant parameter  $\sigma_S$  quantifies the magnitude of random errors in the basin-scale data, which may be caused by (a) inadequacies of the sine wave model and (b) noise in the GRACE mascon inversion (Wiese, Landerer, & Watkins, 2016) quantified by the measurement errors in Figure 3. We assume here that  $\sigma_S$  is unknown and, in Section 5, will compare its estimated value for each basin with the measurement errors in Figure 3.

The value of  $\omega$  is fixed at  $2\pi$  radians per year, yielding a sine wave with a 12-month period, while  $A$ ,  $\sigma_S$ , and  $\delta$  are given vague priors to reflect prior uncertainty in the values of these parameters. Specifically,  $A$  is given a log-normal prior with mode at 30 mm and a CV of 200%,  $\sigma_S$  is given a log-normal prior with mode equal to 10 mm and a CV of 200%, and  $\delta$  is given a flat logit-normal prior between 0 and 1 year with location parameter  $\mu = 0$  and scale parameter  $\sigma = 1.4$ . Note that parameter  $\delta$  represents the phase of the errors; it should not be interpreted as the phase difference between the observed and true signals. For example, if the observed and true signals are in phase, then  $\delta$  will be equal to the shared phase of these signals, not equal to zero.

Note that the sine wave error model does not include a trend correction: it assumes that any long-term increasing or decreasing trend in the GRACE data is representative of the water storage dynamics in the basin. If this assumption is invalid, then this may result in biased posterior estimates for precipitation and evaporation. However, this bias is likely to be relatively small because water storage trends are sensitive to small changes in precipitation and evaporation. For example, a bias of 1 mm in monthly precipitation adds or removes 120 mm of water over a period of 10 years.

While the precipitation and evaporation error models rely on multiple data sets, the use of multiple GRACE solutions (e.g., the CSR mascon solution (Save, 2020) in addition to the JPL solution) may not capture prior uncertainty caused by leakage or scaling errors, since the different solutions are generally limited by the same coarse spatial resolution of the GRACE observations. Therefore, the error model uses a single GRACE solution, that is, JPL mascon data for the results in Section 5 and CSR mascon data for comparison in Section 6.3. Combining multiple GRACE solutions in a single model could still be useful but is not explored in this paper.

## 4. Inference

The probabilistic water balance model described in the previous section defines a joint distribution over the data and all unknown variables, namely the 10 parameters ( $w_p$ ,  $r_p$ ,  $w_E$ ,  $f_E$ ,  $r_E$ ,  $a_Q$ ,  $b_Q$ ,  $\sigma_S$ ,  $A$ , and  $\delta$ ) and the  $4N + 1$  monthly water balance variables ( $S_0$ ,  $P_t$ ,  $E_t$ ,  $Q_t$ , and  $S_t$ ), where  $N$  is the number of months and  $S_0$  is the initial basin water storage at the start of the first month. This paper considers 10 years of data, so  $N = 120$ . Conceptually, we can write the joint distribution of the model as  $p(\mathbf{x}, \boldsymbol{\theta}, \mathbf{S}_{obs})$ , where  $\mathbf{x}$  represents all  $4N + 1$  water balance variables,  $\boldsymbol{\theta}$  is the vector of 10 parameters, and  $\mathbf{S}_{obs}$  represents the entire time series of storage observations. Formally, this distribution depends on the input observations  $P_{obs}$ ,  $E_{obs}$ , and  $Q_{obs}$ , but for notational simplicity this dependence is omitted here.

The goal is now to estimate posterior distributions for  $\mathbf{x}$  and  $\boldsymbol{\theta}$ . The posteriors merge all available information and data, while accounting for all the uncertainties in the model. We first describe the general form of the posteriors and then discuss the specific inference algorithm used.

### 4.1. Posterior Distributions

The posterior for parameter vector  $\boldsymbol{\theta}$  can be written as follows:

$$p(\boldsymbol{\theta} | \mathbf{S}_{obs}) \propto p(\boldsymbol{\theta})p(\mathbf{S}_{obs} | \boldsymbol{\theta}) \quad (17)$$

where  $p(\boldsymbol{\theta})$  is the prior distribution for the parameters and  $p(\mathbf{S}_{obs} | \boldsymbol{\theta})$  is the likelihood. The prior is equal to the product of the individual parameter priors defined in the previous section. The likelihood on the other hand, is obtained by computing the normalizing constant of the conditional water balance posterior  $p(\mathbf{x} | \mathbf{S}_{obs}, \boldsymbol{\theta})$ , as will be shown below.

The likelihood defines a scoring function for the parameters that quantifies how well the storage predicted from the water balance matches the storage observations  $\mathbf{S}_{obs}$ . A good match can generally be achieved by picking bias parameters ( $f_E$ ,  $w_P$ , etc) that move the storage predictions closer to the observations and by making the noise parameters ( $r_E$ ,  $\sigma_S$ , etc) as small as possible: this yields narrow predictive distributions centered on the observations, and thus a large likelihood  $p(\mathbf{S}_{obs}|\boldsymbol{\theta})$  for the parameters. However, since the error parameters are all time-invariant, such near-deterministic predictions generally cannot be achieved for all months simultaneously. A large likelihood is therefore achieved by setting the bias parameters to yield a good match on average across the entire time series and setting the noise parameters just large enough to “capture” all the observations. Clearly, many error parameter combinations may yield a large likelihood; this nonuniqueness is captured by characterizing the entire posterior distribution, rather than only determining the parameters with maximum likelihood or maximum posterior density. As described in the next section, the parameter posterior distribution is estimated using a MCMC algorithm.

The joint posterior for all water balance variables  $\mathbf{x}$  can be written as follows:

$$p(\mathbf{x} | \mathbf{S}_{obs}) = \int p(\mathbf{x} | \mathbf{S}_{obs}, \boldsymbol{\theta}) p(\boldsymbol{\theta} | \mathbf{S}_{obs}) d\boldsymbol{\theta} \quad (18)$$

where  $p(\mathbf{x} | \mathbf{S}_{obs}, \boldsymbol{\theta}) = \frac{p(\mathbf{x}, \mathbf{S}_{obs} | \boldsymbol{\theta})}{p(\mathbf{S}_{obs} | \boldsymbol{\theta})}$  is the posterior distribution of  $\mathbf{x}$ , conditioned on specific values for the parameters. Note that the normalizing constant of this posterior is equal to the parameter likelihood function  $p(\mathbf{S}_{obs}|\boldsymbol{\theta})$  in Equation 17.

Instead of the joint posterior in Equation 18, we are interested in the marginal posterior distributions  $p(x|\mathbf{S}_{obs})$  over individual water balance variables  $x$ , where  $x$  is a scalar variable equal to one of ( $S_0$ ,  $P_t$ ,  $E_t$ ,  $Q_t$ , and  $S_t$ ). For example, if  $x$  corresponds to  $S_t$ , then we aim to compute the posterior distribution for  $S_t$  based on all observations before, on, and after time  $t$ . Such posterior distributions can be computed, as in Equation 18, by averaging conditional posterior distributions  $p(x|\mathbf{S}_{obs}, \boldsymbol{\theta})$  over the parameter posterior distribution  $p(\boldsymbol{\theta}|\mathbf{S}_{obs})$ . An efficient way of computing all the conditional posteriors  $p(x|\mathbf{S}_{obs}, \boldsymbol{\theta})$  is to use a smoothing algorithm, such as a Kalman smoother, as discussed next. Incidentally, a smoothing algorithm also computes the normalizing constant  $p(\mathbf{S}_{obs}|\boldsymbol{\theta})$  of  $p(\mathbf{x}|\mathbf{S}_{obs}, \boldsymbol{\theta})$ , which is used to compute the likelihood in Equation 17 without explicitly constructing the  $(4N + 1)$ -dimensional joint water balance posterior.

#### 4.2. Algorithm

Following the discussion in the previous section, posterior distributions are computed using a double-loop algorithm that combines MCMC sampling for the parameter posteriors with Expectation Propagation (EP) (Minka, 2001), an iterative smoothing algorithm for the water balance posteriors. Essentially, the MCMC algorithm forms an outer loop that iteratively proposes and accepts/rejects new parameter values, while the EP algorithm forms an inner loop that iteratively computes (a) the (unnormalized) posterior density, Equation 17, of parameter values proposed by the MCMC algorithm and (b) the conditional water balance posteriors  $p(x|\mathbf{S}_{obs}, \boldsymbol{\theta})$  for specific parameter vectors sampled by the MCMC algorithm.

For linear-Gaussian models, the EP algorithm is equivalent to a Kalman smoother for  $S_t$  and computes the exact Gaussian water balance posteriors via a single forward-backward pass through the time series, with the backward pass also updating the  $P_t$ ,  $E_t$ , and  $Q_t$  posteriors (see Appendix B). The forward-backward pass ensures that water balance posteriors are estimated using data from the entire time series. Given the values of the error parameters, the probabilistic water balance model in this paper consists of a linear transition model at each time step (i.e., water balance equation, Equation 1) with Gaussian storage observations. However, as discussed in the previous section, the model also uses physical nonnegativity constraints for each  $P_t$ ,  $E_t$ , and  $Q_t$ . These constraints render the input distributions and water balance posteriors non-Gaussian. The EP algorithm used here approximates the exact non-Gaussian water balance posteriors with Gaussian distributions that have the same moments (mean and variance) as the exact posteriors. This strategy is called moment matching. Since the moment matching strategy is applied to the posterior, not the prior, approximations made in one month affect approximations in other months and the algorithm is iterative: instead of a single forward-backward pass, multiple forward-backward passes are used, where each pass further refines the approximations until convergence, that is, until there is no more change in the approximate posteriors.

We implement the probabilistic water balance model in C# using the open-source probabilistic programming library [Infer.NET](#) (Minka et al., 2018). The resulting model code (see Figure A1) uses the [Infer.NET](#) modeling API to implement the model equations listed in the previous section. This code is then automatically translated by the [Infer.NET](#) compiler into the code for running inference, that is, for computing the water balance posteriors with EP (Appendix A).

The MCMC algorithm used in this paper is a single-chain version of the differential evolution MCMC algorithm by ter Braak and Vrugt (2008), which uses a nonparametric proposal (or jumping) distribution based on differential evolution. The algorithm iteratively proposes new parameter vectors and evaluates their posterior density, Equation 17, by calling the EP inference code. The latter computation is done in [Infer.NET](#) by placing the entire model inside a stochastic if block and using EP to compute the posterior odds of being inside versus outside the block, that is, of the model being “true.”

Finally, since the EP algorithm only computes conditional water balance posteriors (conditioned on specific parameter values), a postprocessing step is used that averages computed water balance posteriors over the MCMC sampled parameter sets, as in Equation 18. That way, the final water balance posteriors account for the posterior uncertainty in the data error parameters. For example, if  $p(x|\mathbf{S}_{obs}, \theta)$  represents the (Gaussian) posterior for variable  $x$  (e.g.,  $E_t$ ), conditioned on data  $\mathbf{S}_{obs}$  and on parameter vector  $\theta$ , then the final marginal posterior  $p(x|\mathbf{S}_{obs})$  is computed from  $n$  posterior parameter samples  $\theta_i$  as follows:

$$p(x|\mathbf{S}_{obs}) = \int p(x|\mathbf{S}_{obs}, \theta)p(\theta|\mathbf{S}_{obs})d\theta \approx \frac{1}{n} \sum_{i=1}^n p(x|\mathbf{S}_{obs}, \theta_i) \quad (19)$$

As such, each marginal water balance posterior is strictly speaking a (Gaussian) mixture distribution, although empirically it turns out to be well approximated by a single Gaussian distribution using moment matching. While this last approximation is not strictly necessary, it avoids storing the entire Monte Carlo mixture (for each water balance variable and each month).

## 5. Results

First, detailed results are presented for one of the basins (Mond), followed by a summary of the results for all the basins. Detailed results for all the basins are available in the supporting information.

### 5.1. Mond Basin

Mond basin is one of the drier basins in this study (Table 1) with significant prior uncertainty in evaporation (Figure 2). Water balance posteriors for Mond basin are shown in Figure 4 and error parameter posteriors are shown in Figure 5. In Figure 4, the estimated precipitation tends to more closely follow the CHIRPS data than the IMERG data, especially during the wet winter months, with IMERG apparently overestimating the precipitation. This is reflected in the inferred value for parameter  $w_p$  (last row in Figure 4), which is shifted toward 1, indicating greater weight on CHIRPS than on IMERG for this basin. The wide posterior for noise scaling parameter  $r_p$  indicates that this parameter does not play an important role here, and the posterior uncertainty in precipitation is not markedly different from the prior uncertainty shown in Figure 2.

In contrast, the posterior uncertainty in evaporation is significantly smaller than its prior uncertainty, as shown by the posterior uncertainty bands in Figure 4 (second row) and posterior values of  $r_E < 0.5$ , indicating that random errors in evaporation are smaller than the absolute difference between the SSEBop and GLEAM data. The estimated evaporation lies more or less right between the two data sets, with an estimated  $w_E$  value around 0.5 (equal weights) and no additional bias ( $f_E$  around 1). Posterior uncertainty increases during dry summers when the differences between the two data sets are largest.

River discharge in this basin is an order of magnitude smaller than the other water balance variables. With the assumed 10% relative error, this results in small posterior uncertainty that closely follows prior uncertainty (third row in Figure 4). Note, however, the significant increase in discharge uncertainty at the end of the time series: no river discharge observations are available in the basin for the last 3 months of 2015, and the historical discharge variability is instead used as the prior for these months, as discussed in Section 4.

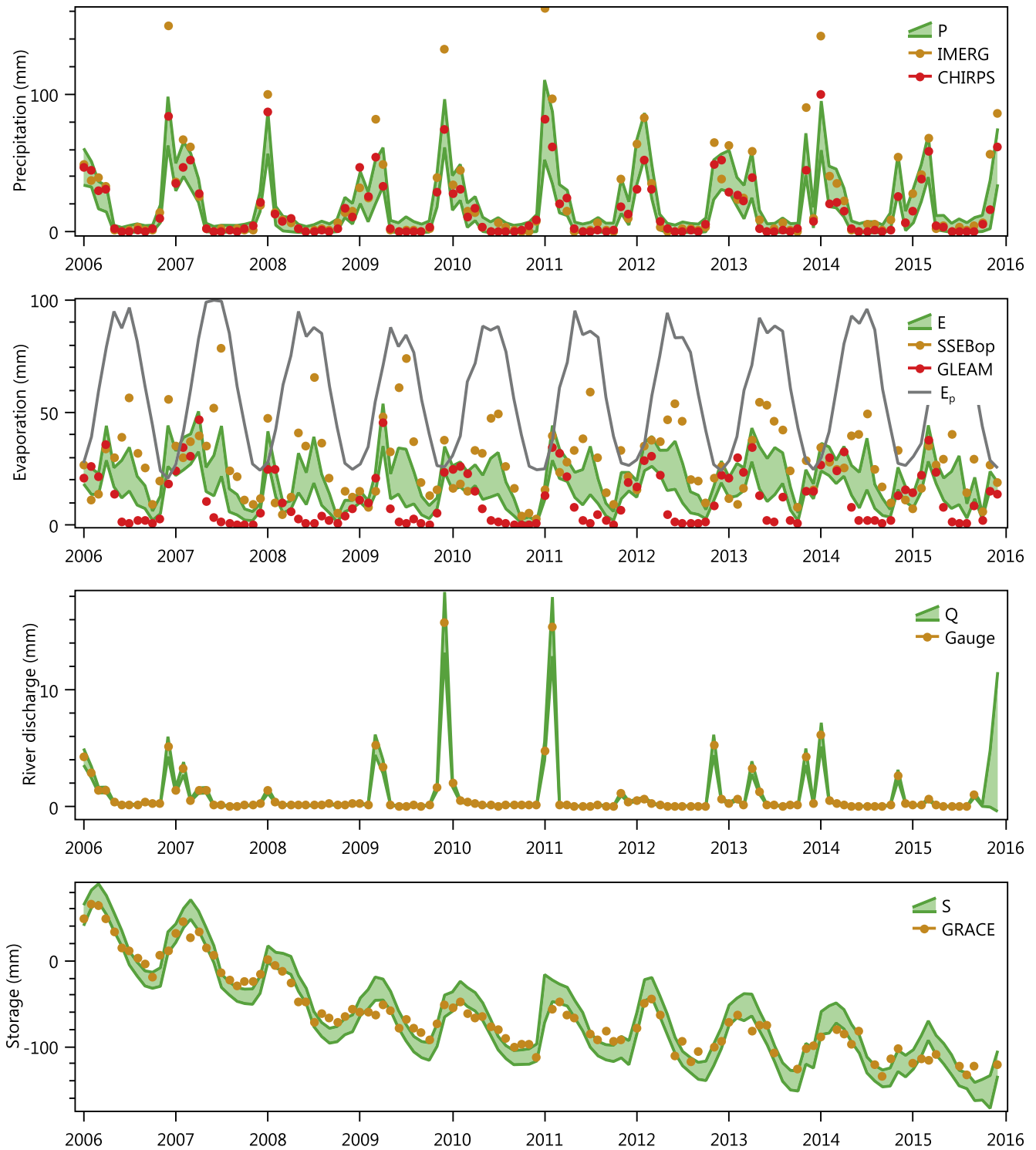


**Figure 4.** Monthly water balance estimates for Mond basin, shown as 90% posterior uncertainty bands. Each year label indicates the start of the year (January). All values are in mm/month.

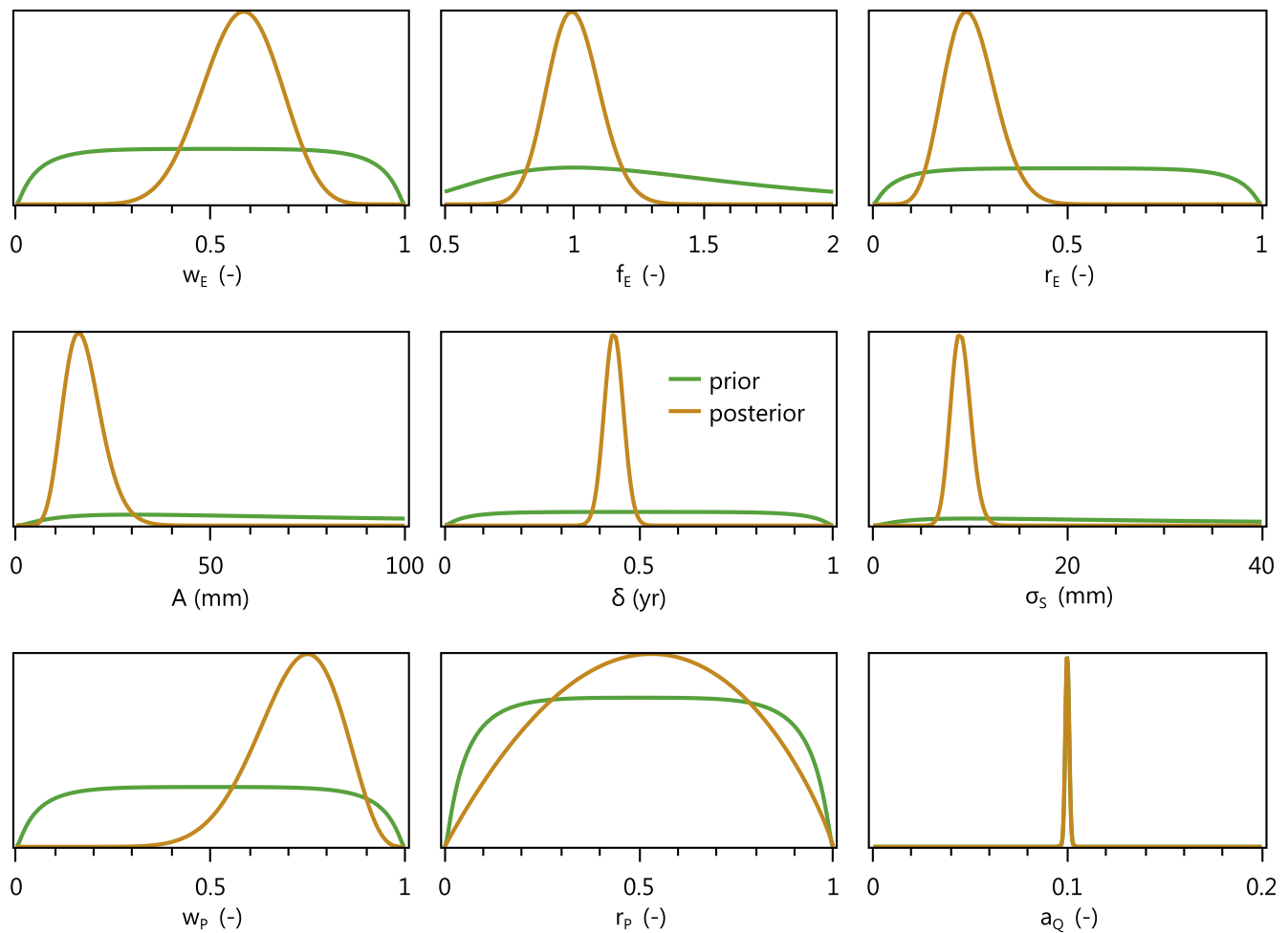


**Figure 5.** Normalized prior and posterior densities of error parameters for Mond basin.

The larger posterior uncertainty in discharge for these months does not appear to affect the uncertainty in the other water balance components. This will be further explored in Section 6.

The last row of Figure 4 shows that the inferred water storage dynamics largely follow the GRACE observations, with a small increase in seasonal amplitude in the posteriors compared to the data. The corresponding inferred storage error parameters are shown in the second row of Figure 5. All three parameters ( $A$ ,  $\delta$ , and  $\sigma_S$ ) have well defined posterior distributions compared to their vague priors. Residual noise in the data, after making amplitude ( $A$ ) and phase adjustments ( $\delta$ ), is relatively small as indicated by an inferred value for  $\sigma_S$  of around 10 mm. Note that inferred posteriors for months with missing GRACE observations (e.g., May–June 2015, October–November 2015) do not markedly differ from months with observations. This is because error parameter values learned from months with data are shared across all months and because smoothing infers posteriors using data from all months. A more dramatic example of this effect will be seen in Section 6.

## 5.2. Other Basins

The Supporting Information contains posterior plots for all other basins, similar to the ones for Mond basin shown above. Here, we highlight the main findings from these results. All basins exhibit long-term declining trends in water storage, as found in other regions across Iran (Khaki et al., 2018). In terms of water storage posteriors, the basins can roughly be divided into basins without a significant change in amplitude or phase between the estimated posteriors and the GRACE data (Mond, Karoon, and Karkheh), basins with

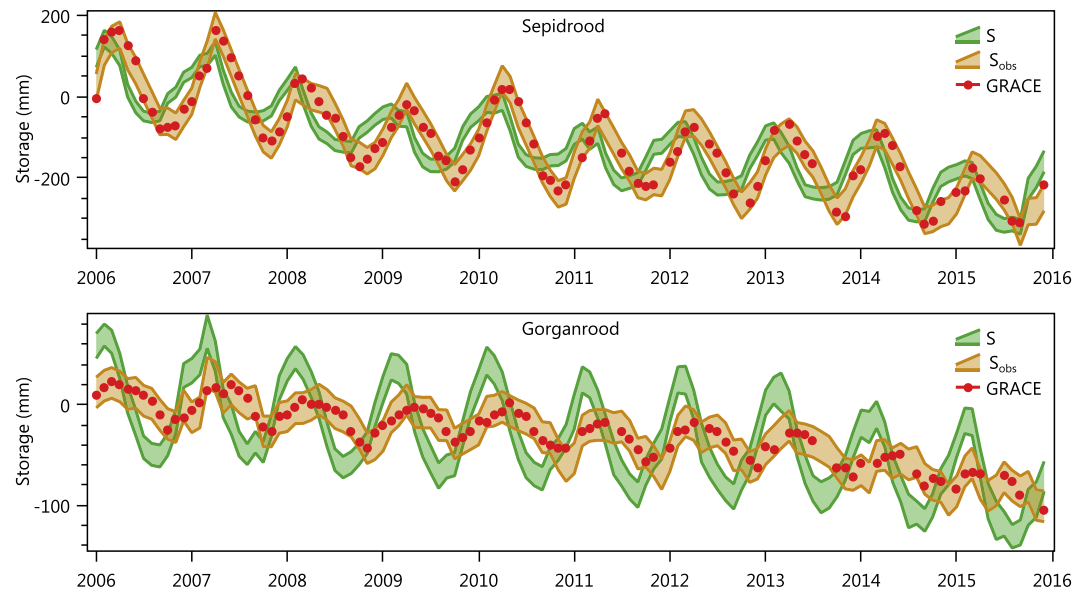


**Figure 6.** Ninety percent uncertainty bands of storage posteriors ( $S$ ) and GRACE posterior predictive distributions ( $S_{obs}$ ), along with GRACE data for Sepidrood and Gorganrood basins.

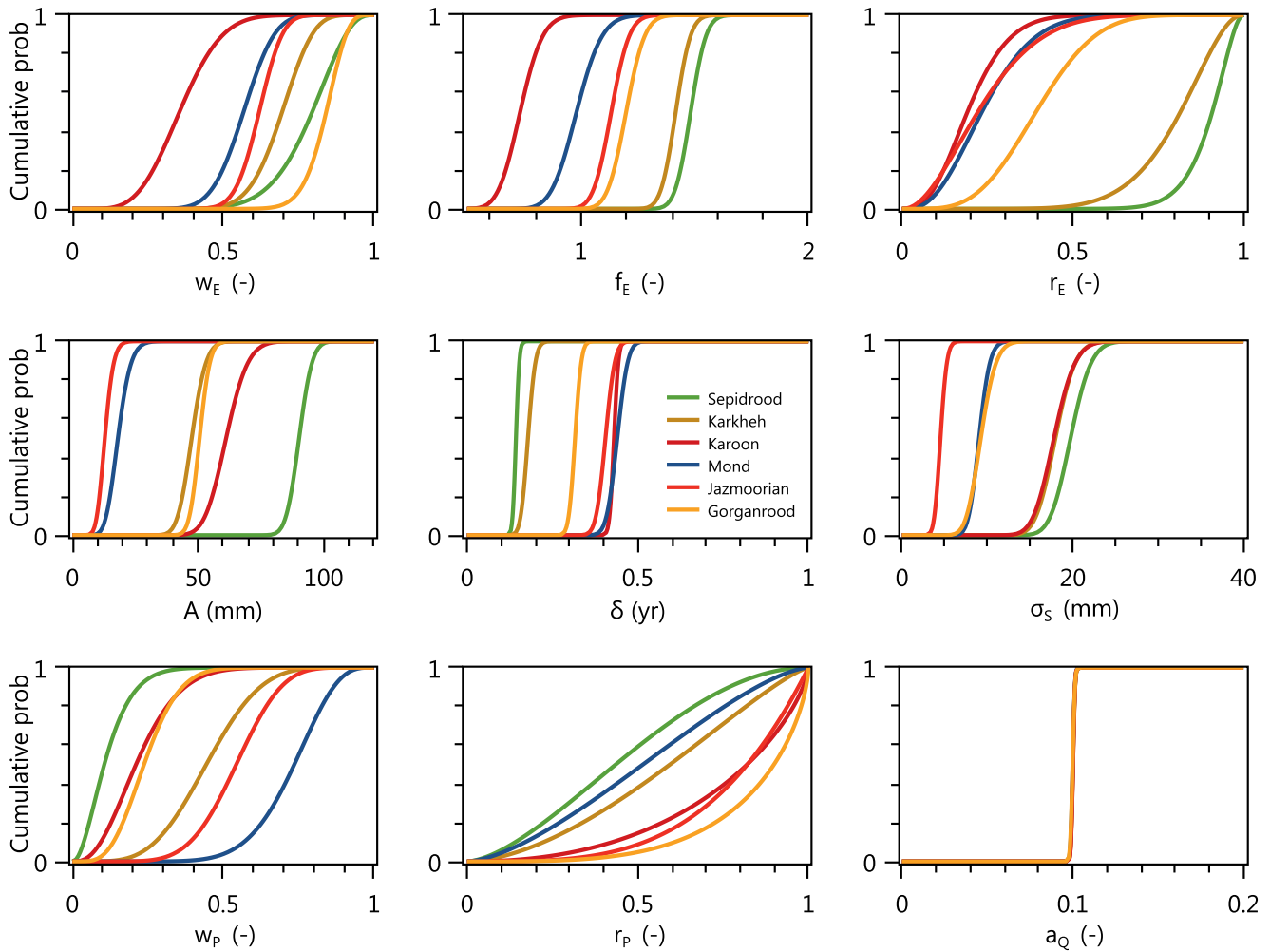
only a change in phase (Sepidrood), basins with only a change in amplitude (Jazmoorian), and basins with both a change in amplitude and phase (Gorganrood).

Figure 6 illustrates this for the Sepidrood and Gorganrood basins. In both basins the inferred storage dynamics (posteriors shown in green) are shifted earlier in time than the corresponding GRACE observations. Apparently, the observed GRACE dynamics do not fit with the other water balance observations in terms of water balance closure. Interestingly, both basins are in the north of the country where the large footprint of the GRACE observations (Figure 3) is possibly affected by the Caspian Sea to the north, which is not included in the CRI filter of the JPL GRACE data set and whose seasonal water level dynamics are shifted in time compared to Sepidrood and Gorganrood basins (Forootan et al., 2014); see also Figure S18. J. Chen et al. (2017) observed leakage of GRACE signals from the Caspian Sea into surrounding land areas, and this may explain the bias in the phase and amplitude of the GRACE water storage dynamics seen in Figure 6. For the basins investigated here, the sine wave error model appears to restore the underlying water storage dynamics (Figure 6), including an increase in amplitude for the relatively small Gorganrood basin. The increase in amplitude can be explained by the strong spatial smoothing inherent in the coarse-scale GRACE data, which tends to be more severe in smaller basins.

Figure 6 also shows posterior predictive distributions for the GRACE observations ( $S_{obs}$ ) conditioned on the posterior mean of the true water storage ( $S$ ). These plots illustrate the validity of the proposed sine wave model, since the original GRACE observations fall within the posterior predictive distributions obtained by taking the inferred posterior mean of  $S_t$  in each month and applying the noisy sine wave model to generate a predictive distribution for the corresponding observation  $S_{obs,t}$ . This however does not mean that the probabilistic water balance model is generally suitable for making water balance predictions, as will be illustrated in Section 6.

Error parameter posterior distributions for all basins are shown in Figure 7. The third row in this figure shows that for most basins IMERG fits better with the other water balance data than CHIRPS, since inferred values for  $w_p$  are mostly less than 0.5 (more weight on IMERG). Mond basin is the exception, with  $w_p > 0.5$ , as discussed above. The insensitivity of parameter  $r_p$  that was already observed in Mond basin, also occurs in two other basins (Sepidrood and Karkheh), while in the three other basins  $r_p$  does matter and tends toward a value of 1.

The three evaporation error parameters are mostly well identified (first row in Figure 7). In most basins, more weight is given to the GLEAM data set ( $w_E > 0.5$ ), with the exception of the wettest basin (Karoon)



**Figure 7.** Posterior error parameter distributions for all basins.

where SSEBop provides a better fit. However, in all basins a weighted average of the two data sets is preferred over using either data set alone. Inferred values for bias parameter  $f_E$  range between 0.5 and 1.5, with the largest values for Karkheh and Sepidrood basins. While a multiplicative bias of 1.5 may seem excessive, the inferred evaporation posteriors remain at or below the potential evaporation (see supporting information), even though potential evaporation was not used in the model. Finally, the reduction in prior evaporation uncertainty found in Mond basin also occurs in other basins, as evidenced by inferred values for  $r_E$  below 0.5, with the exception of Karkheh and Sepidrood basins where prior evaporation uncertainty is less pronounced than in the other basins.

The storage error parameters (second row in Figure 7) are also well identified in all basins. Standard deviation  $\sigma_S$  of random errors in the GRACE observations, after amplitude and phase corrections, is 10 mm or less for the drier basins in the east (Mond, Jazmoorian, and Gorganrood) and 15–20 mm for the wetter basins in the west (Sepidrood, Karkheh, and Karoon). As shown in Figure 8, the estimated posterior mean values for  $\sigma_S$  closely follow a similar west to east decreasing trend as the JPL-mascon GRACE measurement errors, with an increase in estimated noise for the smaller Gorganrood basin. These results suggest that the sine wave model adequately captured and corrected the systematic errors in the GRACE data due to a mismatch in scale, yielding random errors similar to and even smaller than the reported GRACE measurement errors.

Finally, Table 3 summarizes and compares the posterior standard deviations for the different water balance variables. The table includes results for a second scenario with vague prior on  $a_Q$ , which is further discussed in Section 6. Results in this table show that posterior uncertainty, in terms of posterior standard deviation,

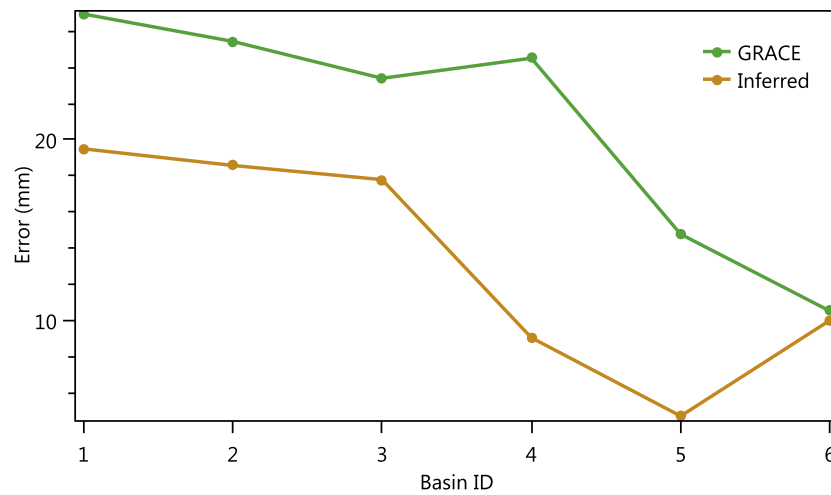


**Figure 8.** Posterior mean of  $\sigma_s$  compared to mascon-scale standard error of the JPL GRACE observations.

tion, decreases from water storage (4–12 mm/month), to precipitation (3.5–7 mm/month), to evaporation (2–6 mm/month), and to discharge (0–2 mm/month). The small posterior uncertainty in river discharge is a direct consequence of the assumed 10% error and the generally small discharge values in the semi-arid basins studied here. At the extreme end, the endorheic Jazmoorian basin has no outflow, and thus zero discharge and error.

The reported posterior standard deviations result from the fusion of all water balance data. For example, the posterior of  $S_t$  in a particular month  $t$  results from the fusion of three noisy information streams: the GRACE observation for that month (if not missing), the water balance constraint for month  $t$ , and the water balance constraint for month  $t + 1$ , for which  $S_t$  provides the initial storage. A combination of these three information streams results in a posterior that is narrower (less uncertainty) than any of the individual streams, with each stream or distribution more or less constraining the final posterior estimate of  $S_t$ . A similar process happens when inferring the other water balance variables ( $P_t$ ,  $E_t$ , and  $Q_t$ ), although for those variables only two information streams are involved (one from the prior and the other from the water balance for month  $t$ ).

## 6. Discussion

This section evaluates how the results are affected when changing some of the data and assumptions of the probabilistic water balance model.

### 6.1. Sensitivity to Assumed River Discharge Errors

Results in the previous section were based on a narrow prior for the relative error  $a_Q$  of monthly river discharge data centered on 0.1 (10%). To test the sensitivity of the results to this choice, an alternative vague log-normal prior for  $a_Q$  was used, that is, one with mode at 0.1 and with a coefficient of variation of 0.9. Table 3 shows that this change increases the estimated posterior standard deviation of the monthly river discharge but has otherwise little effect on posterior uncertainty and the estimates of the other water balance variables. The largest absolute increase in the estimated standard deviation of  $Q$  is observed for Karoon basin, which is the wettest basin included in the analysis. In fact, for Karoon basin, the posterior standard deviation of river discharge becomes larger than that of evaporation (Table 3).

**Table 3**  
Average Posterior Standard Deviation (mm/month) of Each Water Balance Variable for Two Cases: (a) Relative River Discharge Error  $a_Q$  Fixed at 0.1 (10%) and (b) a Vague Lognormal Prior for  $a_Q$  With Mode at 0.1 and CV Equal to 0.9

Basin	$a_Q = 0.1$				Vague prior on $a_Q$			
	$P$	$E$	$Q$	$S$	$P$	$E$	$Q$	$S$
Sepidrood	6.0	5.1	0.2	10.1	6.0	5.1	0.4	10.1
Karkheh	6.1	6.1	0.4	11.2	6.2	6.1	1.0	11.1
Karoon	6.9	4.8	1.7	11.3	6.8	4.6	5.6	11.7
Mond	4.7	3.5	0.1	6.7	4.7	3.6	0.3	6.8
Jazmoorian	3.5	1.9	0.0	4.1	3.5	1.9	0.0	4.0
Gorganrood	6.7	4.9	0.2	8.3	6.8	5.0	0.4	8.3

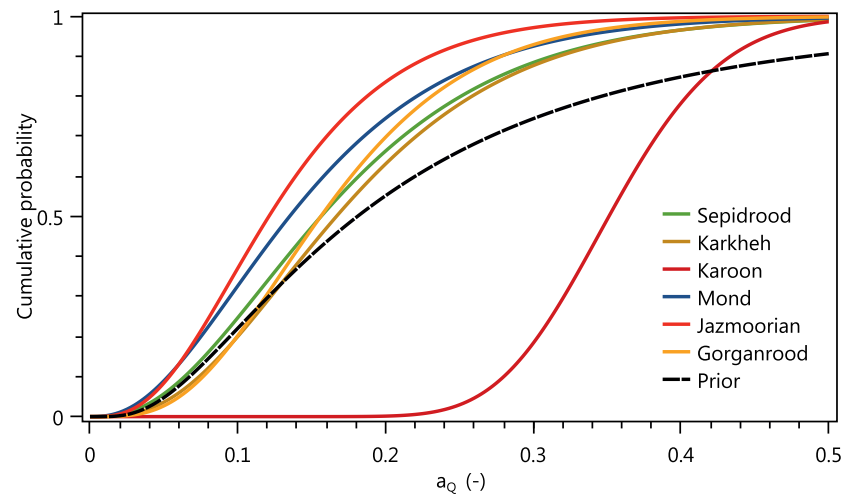


**Figure 9.** Posterior distributions (CDF) for  $a_Q$  when using a vague prior (dashed) for  $a_Q$ .

When using a vague prior, posterior distributions for relative error  $a_Q$  in Figure 9 show that the posteriors are generally close to the prior. Most basins show a slight contraction of the posterior relative to the prior toward smaller relative errors, with the exception of Karoon basin where the posterior moves to larger, likely unrealistic, values for  $a_Q$  around 0.3–0.4. These large values suggest that uncertainty in river discharge increases to compensate for errors somewhere else in the water balance. Due to the small magnitude of river discharge relative to the other water balance terms, a large relative error is needed to get a sizable effect.

These results indicate that for the semiarid basins studied here, the value of  $a_Q$  cannot be estimated reliably from the water balance data and instead, river discharge errors should be estimated independently, for example, using a formal rating curve error analysis (Horner et al., 2018; Kiang et al., 2018). The value of  $a_Q$  can then be fixed a priori or given a narrow prior, based on the independent estimate. On the other hand, accurate estimates of  $a_Q$  are only relevant for estimating uncertainty of the river discharge data. For the goal of estimating the other water balance variables, approximate estimates of  $a_Q$  suffice, at least when river discharge is the smallest term in the water balance.

## 6.2. Effect of Missing GRACE Observations

Results in Section 5 already showed that missing GRACE observations do not significantly affect the inferred posteriors. Sharing of error parameters across the entire time series, combined with the fusion of all data via smoothing, allows the model to fill in occasional gaps in the data record. It is however instructive to evaluate a few more drastic scenarios of missing GRACE observations to gain additional insight into the predictive capabilities and limitations of the probabilistic water balance model.

Two fictitious scenarios are evaluated. The first scenario assumes that all GRACE observations after 2010 are missing; the first 5 years provide a complete data record to learn the model error parameters, which are then applied to infer and predict storage posteriors in the next 5 years. Figure 10 shows that in the absence of constraining GRACE observations in the second part of the period, posterior uncertainty grows over time and an increasing trend in storage is (wrongly) predicted. In the second scenario, which assumes a single annual observation is available after 2010, this trend is removed and posterior uncertainty is smaller, although it remains larger than when the full GRACE observation record is used.

These results illustrate that the model is less suitable for long-range predictions without storage observations: uncertainties quickly accumulate and small imbalances between precipitation and evaporation easily lead to erroneous trend predictions. On the other hand, the model works well for interpolating and filling in gaps when observations are occasionally missing.

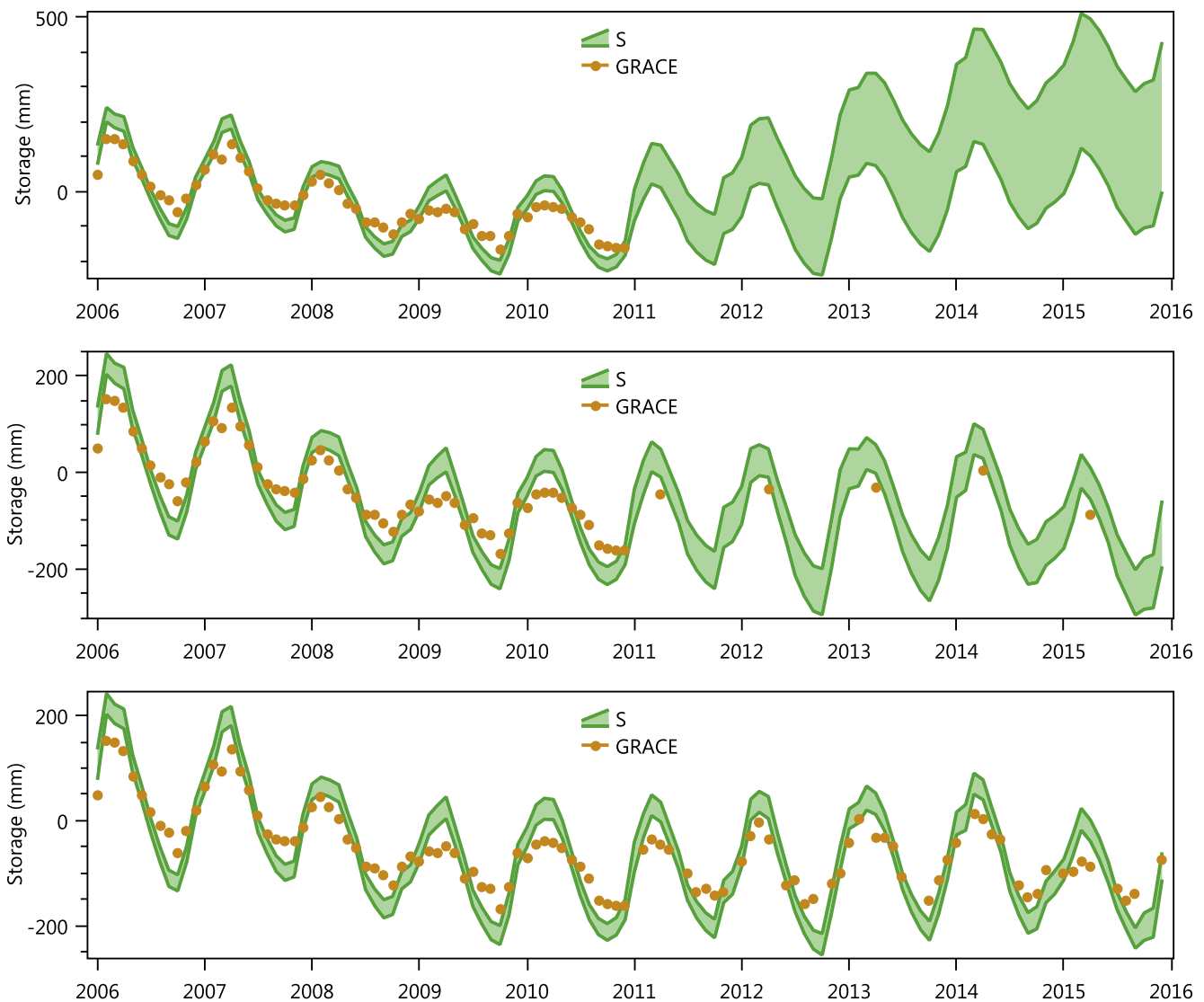


**Figure 10.** Storage posteriors for Karoon basin for three scenarios of missing GRACE observations: (a) no GRACE observations in the last 5 years, (b) one GRACE observation per year in the last 5 years, and (c) using all available observations.

### 6.3. Using a Different GRACE Solution

The results in this paper are based on the JPL-mascon GRACE data. The model can also use other GRACE solutions by simply replacing  $S_{obs}$  in the model by another data set. Figure 11 compares inferred posterior distributions for  $\sigma_S$  when using the CSR mascon solution instead of the JPL mascon solution. For the basins studied in this paper, the JPL data consistently yield smaller noise, that is, smaller posterior values for  $\sigma_S$ . This indicates that the JPL data provide a better fit with the other monthly water balance data used in this study, at least after bias correction. The larger estimated noise in the CSR data is also apparent in the time series plots shown in Figure S15.

### 6.4. Effect of Positivity Constraints

As described in Section 4, the model includes positivity constraints on water balance variables  $P$ ,  $E$ , and  $Q$ , since these variables cannot physically be negative. To what extent do these constraints affect the inferred posteriors? This can be assessed by removing the positivity constraints from the model, which is achieved by commenting out the three Variable.ConstrainPositive statements in Figure A1 and recomputing the posteriors.

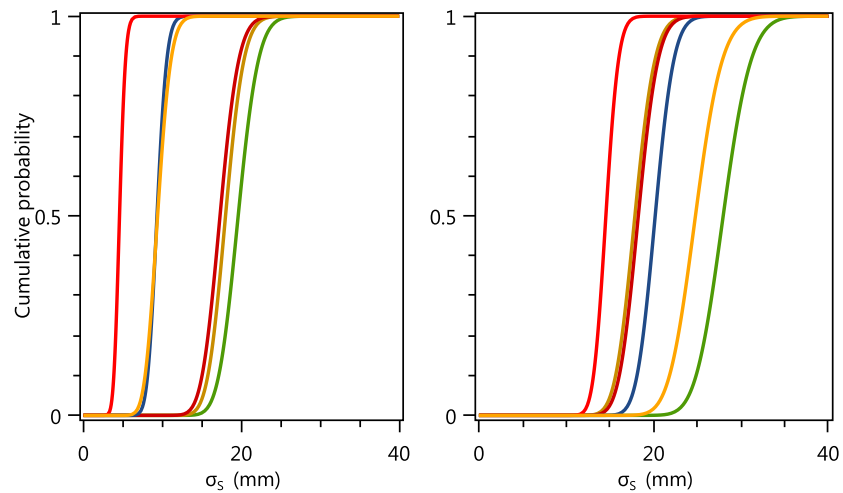


**Figure 11.** Posterior distributions (CDF) of  $\sigma_s$  for two different GRACE mascon solutions: JPL (left) and CSR (right).

Conditional on the model parameters, the model now only contains Gaussian and linear relations. As such, inference does not require any iteration and a single forward-backward pass over the monthly time series is sufficient to compute all water balance posteriors. The [Infer.NET](#) compiler, in fact, automatically detects this and, in the absence of positivity constraints, generates an inference code that is equivalent to a Kalman smoother.

Figure 12 shows that constraining the water balance variables to be positive results in smaller posterior uncertainty when the unconstrained posterior extends into the negative domain. In this case (Karkheh basin), the unconstrained evaporation posterior has a negative tail whenever there is a large difference between the two evaporation data sets (e.g., summer 2009) because then, the (prior) uncertainty is large. However, overall, for the basins analyzed here, the effect of the positivity constraints is fairly limited and does not significantly change the results. This is also why the number of EP iterations to achieve convergence is small (we used three iterations); the studied problems are only mildly non-Gaussian. However, the positivity constraints do maintain physically realistic posteriors and thus are useful for the general applicability of the model.

### 6.5. Alternative Data Error Models

The methodology presented in this paper relies on explicit assumptions about the data errors in the form of parametric error models. Section 3 presents a possible, but certainly not unique, set of models and assumptions. The validity of the data error assumptions can be checked by (a) evaluating whether the estimated water balance variables and parameters are reasonable and consistent with the prior assumptions and (b) how well the model fits the data.

For example, for precipitation, this means that the estimates should lie in between the two precipitation data sets, since the model in Equation 2 interpolates between the two data sets. Time series plots of estimated precipitation (Figure 4 and supporting information) show that this is indeed generally the case for the basins studied here. For basins where posterior estimates deviate from this assumption or where it is difficult to close the water balance, it may be necessary to either use different precipitation data sets or to use a precipitation error model that includes an additional bias parameter (e.g., similar to what is used in the paper for the evaporation error model).

Another set of assumptions adopted in this paper is that, due to spatial and temporal scale differences, basin-scale water storage data based on GRACE may have both phase and amplitude errors, in addition to random errors. These assumptions led to the noisy sine wave error model proposed in Section 3.4. Figure 6 showed two basins (Sepidrood and Gorganrood) with such phase and amplitude errors. We then evaluate two alternative data error models for these basins and compare them to the noisy sine wave error model proposed in this paper.

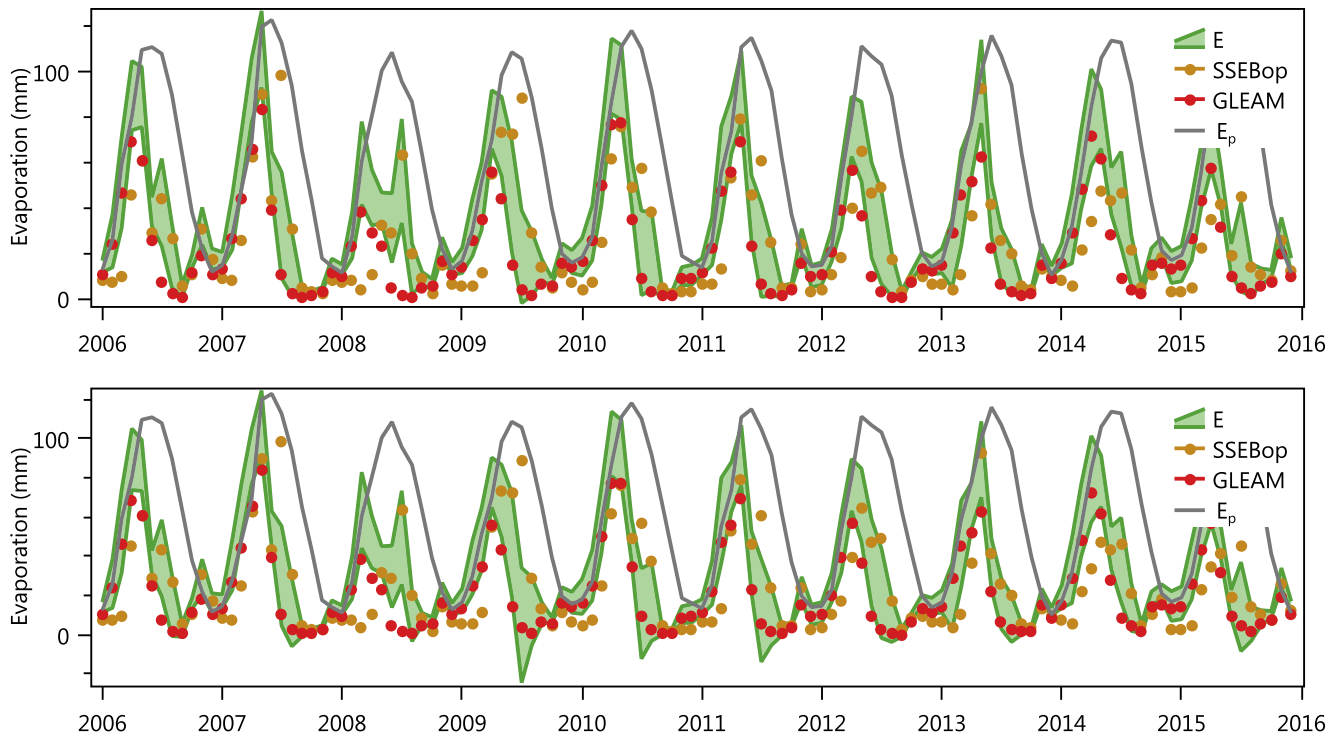


**Figure 12.** Posterior 90% uncertainty bands for monthly evaporation in Karkheh basin with (top) and without (bottom) positivity constraints in the model.

Figure 13 shows water storage estimates for Sepidrood basin using three different GRACE data error models. The bottom plot is the same as in Figure 6 and is based on the noisy sine wave error model. The top and middle plots use GRACE data scaling factors from the JPL mascon data set to account for amplitude errors but assume no phase errors (no lags or shifts). The scaling factors are based on simulations with the Community Land Model to downscale the data to a half-degree grid (Wiese, Landerer, & Watkins, 2016). The top plot fixes the standard deviation  $\sigma_s$  of the random errors to the value in the JPL mascon data set (as in Figure 3), while the middle plot estimates  $\sigma_s$  from the water balance data. Results in Figure 13 show that assuming no phase errors (top, middle) leads to posterior predictions of storage observations ( $S_{obs}$ ) that either do not overlap with the data (top) or lead to wide prediction bands (middle). Consequently, the two models without phase errors have significantly lower likelihood ( $-669$  and  $-593$ ) than the noisy sine wave error model (bottom) that includes phase errors (likelihood  $-514$ ).

Similar results are obtained for Gorganrood basin (Figures S16 and S17), where the noisy sine wave model again gives the best match with the data (highest likelihood of  $-466$  vs.  $-559$  and  $-595$  for the two other models). The first model without phase error and fixed  $\sigma_s$  leads to a good match with the GRACE observations due to the small value for  $\sigma_s$  (Figure S16) but a worse match for the precipitation and especially the evaporation data, whose estimates now have to be adjusted to close the water balance. Estimating  $\sigma_s$  from the data in the second model without phase error leads to an increase in  $\sigma_s$  and a phase shift in the estimated storage values (Figure S17), which is in conflict with the assumptions of this model (no phase error).

These results suggest that the estimated amplitude and phase errors in Figure 6 may be real, although the estimates in principle still depend on the chosen precipitation and evaporation data and error models. Phase errors (time lags) of 1–2 months have also been observed in studies comparing GRACE data to terrestrial water storage simulated with hydrological models (Biancamaria et al., 2019; Döll et al., 2014; Scanlon, Zhang, Rateb, et al., 2019; Schmidt et al., 2008; L. Zhang et al., 2017). Whereas some of these studies have attributed the lag between observed and simulated water storage to model errors, our results suggest that data errors also play a role. Since the methodology in this paper does not rely on a hydrological model, it can help pinpoint the source of data-model mismatches. For this to work correctly, however, the methodology requires appropriate data and error models for precipitation and evaporation (and discharge). While the

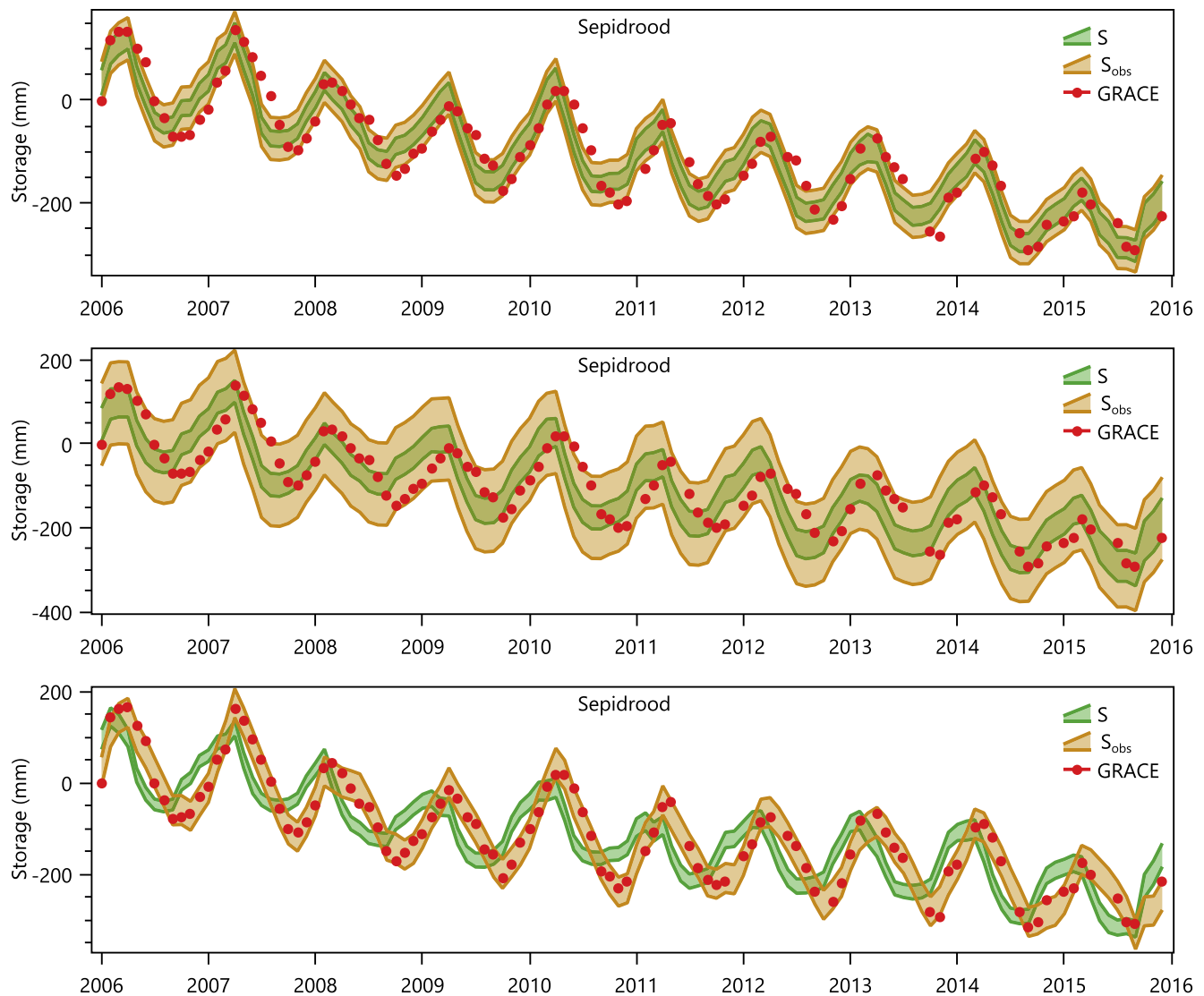


**Figure 13.** Posterior water storage estimates for Sepidrood basin using three different data error models. The top and middle plots are for a model that assumes no phase errors and with the standard deviation of the random errors either fixed (top) or estimated from the data (middle). The bottom plot uses the noisy sine wave error model in Section 3.4 (same plot as in Figure 6).

data error models in Section 3 generally work well for the basins studied in this paper, it is important to evaluate and possibly modify these models for other basins. The model implementation used in this paper makes it straightforward to compare different error models and data sets and to extend the approach, for example, by including additional data sets for precipitation and evaporation.

## 7. Conclusions

The paper presents a probabilistic model to estimate monthly basin-scale precipitation, evaporation, terrestrial water storage, and river discharge based on independent observations of each water balance term and monthly water balance constraints. The main contribution compared to previous water balance fusion studies is that data errors are not fixed a priori but are treated as unknown random variables that are estimated from the data. This results in a data fusion approach that combines data error and water balance estimation into a single coherent methodology.

The approach is based on formulating a Bayesian hierarchical model that ties together all data, water balance variables and data error parameters, followed by computing the posteriors of all unknown parameters and water balance variables in the model. The model combines monthly basin-scale water balance constraints with data error models for each water balance variable (precipitation, evaporation, river discharge, and water storage) that account for random and systematic data errors.

Specifically, bias in precipitation and evaporation data is modeled as a weighted average of two different data sets (IMERG and CHIRPS for precipitation and SSEBop and GLEAM for evaporation), where the weight is treated as an unknown parameter. For evaporation, a second unknown bias parameter is included for additional flexibility in modeling bias. Random errors in precipitation and evaporation are modeled as a function of differences between the two respective data sets, with unknown parameters controlling the magnitude of the random errors. The JPL-mascon GRACE data are used as basin-scale water storage observations. Measurement and scaling errors in the GRACE data are described by a noisy sine wave error model, with amplitude, phase, and noise of the sine wave controlled by unknown parameters. Finally, monthly river discharge data are taken from river gauging stations, with random errors described by a relative error parameter.

The resulting probabilistic model is solved for the unknown water balance variables and data error parameters using MCMC sampling (for the parameters) in combination with an iterative smoothing algorithm (for the water balance variables) that maintains the nonnegativity of the water balance variables. Computed posteriors provide (a) hydrologically consistent, error-filtered and bias-corrected water balance estimates and (b) statistically consistent, basin-specific error estimates of the water balance data.

Application to semiarid river basins in Iran illustrates the usefulness of the approach. First, computed evaporation posteriors achieve significant reductions in prior evaporation uncertainty during water-stressed summers. Other studies have also reported reductions in errors by combining multiple evaporation products (Hobeichi, Abramowitz, Evans, & Ukkola, 2018; Mueller et al., 2011). Second, the approach leads to basin-specific phase and amplitude corrections of the GRACE data and is able to extract the underlying water storage dynamics. Third, by fusing all water balance data, posterior water balance estimates are obtained with time-averaged standard errors of 4–12 mm/month for water storage, 3.5–7 mm/month for precipitation, 2–6 mm/month for evaporation, and 0–2 mm/month for river discharge. Data error parameters are generally well identified, with the exception of the relative error in the river discharge data, which is best estimated using an independent rating curve analysis. This lack of sensitivity, however, also means that the other water balance estimates are not strongly affected by the assumed discharge errors, and an approximate estimate suffices as long as river discharge is the smallest term in the water balance, as is the case for the semiarid basins studied here.

The proposed methodology is data-driven in that no hydrological process assumptions are made beyond the monthly water balance constraints. As such, the water balance posteriors can be used for independent evaluation and calibration of monthly water balance models. Nevertheless, an interesting extension could be to embed the data errors models used here into a monthly water balance model, and to perform joint estimation of all error and hydrological parameters. Another modification would be to consider spatially distributed error models, for example, using land cover specific error models for evaporation and elevation or temperature specific error models for precipitation, and sharing these parameters across multiple basins to ensure identifiability.

The approach can also be extended to other data sets and other (gauged) basins around the world, possibly using tailor-made data error models. Modifications may be warranted to describe data errors in different climates and landscapes, for example, in snow-dominated basins, where satellite data may underestimate snow accumulation. A benefit in this respect is that the model is implemented in a general-purpose and extensible probabilistic programming tool ([Infer.NET](#)) that separates model assumptions from inference (model solving): when the individual data error models are modified, the inference code is automatically generated to compute posteriors for the new model.

## Appendix A: Implementation of the Probabilistic Water Balance Model in Infer.NET

Figure A1 shows how the probabilistic water balance model in Section 3 translates directly into a probabilistic program implemented with the Infer.NET modeling API. The Infer.NET compiler automatically trans-

```
// Time loop
using (var time = Variable.Each(timeInterval))
{
    var t = time.Index;

    // P
    var mP = (1 - wP) * PObs1[t] + wP * PObs2[t];
    var sP = Variable.Max(PStd[t], rP * 0.5 * Abs(PObs1[t] - PObs2[t]));
    P[t] = Variable.GaussianFromMeanAndVariance(mP, sP * sP);
    Variable.ConstrainPositive(P[t]);

    // E
    var mE = fE * ((1 - wE) * EObs1[t] + wE * EObs2[t]);
    var sE = Variable.Max(0.1 * mE, rE * 0.5 * Abs(EObs1[t] - EObs2[t]));
    E[t] = Variable.GaussianFromMeanAndVariance(mE, sE * sE);
    Variable.ConstrainPositive(E[t]);

    // Q
    var mQ = Variable.GaussianFromMeanAndVariance(QObs[t], QObsVar[t]);
    var sQ = aQ * QObs[t] + bQ;
    Q[t] = Variable.GaussianFromMeanAndVariance(mQ, sQ * sQ);
    Variable.ConstrainPositive(Q[t]);

    // S: water balance
    using (Variable.If(t == 0))
    {
        S[t] = S0 + P[t] - E[t] - Q[t];
    }
    using (Variable.If(t > 0))
    {
        S[t] = S[t - 1] + P[t] - E[t] - Q[t];
    }

    // SObs
    var missingSObs = IsNaN(SObs[t]);
    using (Variable.IfNot(missingSObs))
    {
        const double omega = 2 * Math.PI;
        var mS = S[t] + A * Sin(omega * (Variable.Double(t) / 12 - Delta));
        var sS = SStd;
        SObs[t] = Variable.GaussianFromMeanAndVariance(mS, sS * sS);
    }
}
}
```

Figure A1. Implementation of the probabilistic water balance model using the Infer.NET probabilistic programming API in C#.

lates the model code into an iterative smoothing algorithm for computing water balance posteriors using Expectation Propagation (EP). The complete code is at <http://doi.org/10.5281/zenodo.4116451>.

## Appendix B: Details of EP

Here, we give details of how EP computes conditional water balance posteriors. EP uses “messages,” that is, Gaussian distributions in this case, to propagate the uncertainty through the model. If we write the water balance at each time as  $S = S_0 + P - E - Q$  (omitting the time index for simplicity), then the forward message (Gaussian distribution) to  $S$  is computed by propagating Gaussian distributions for the inputs ( $S_0$ ,  $P$ ,  $E$ ,  $Q$ ) through the water balance:

$$\text{forward message to } S = \mathcal{N}(S | m_{S_0} + m_P - m_E - m_Q, v_{S_0} + v_P + v_E + v_Q) \quad (\text{B1})$$

where  $m_x$  and  $v_x$  represent the mean and variance of input  $x$ . The mean and variance of  $P$ ,  $E$ , and  $Q$  are given by the model priors described in Section 3, modified for truncation at zero, see below. The mean and variance of previous storage  $S_0$  is given by multiplying two Gaussian distributions: the forward message that was sent to  $S_0$  in the previous time step and the Gaussian likelihood of a GRACE observation, if any. The mean and variance of the resulting Gaussian message (distribution) is given by the general Gaussian multiplication formula:

$$\mathcal{N}(x | m_1, v_1) \mathcal{N}(x | m_2, v_2) \propto \mathcal{N}(x | m, v) \quad (\text{B2})$$

$$m = w_2 m_1 + w_1 m_2 \quad (\text{B3})$$

$$v = w_2 v_1 + w_1 v_2 \quad (\text{B4})$$

where  $w_1 = \frac{v_1}{v_1 + v_2}$ ,  $w_2 = \frac{v_2}{v_1 + v_2}$ , and  $x$  in this case would be  $S_0$ . This formula is the scalar version of the

Kalman filter update equation. Forward messages are computed by a forward pass through the entire time series.

Likewise, backward messages represent (Gaussian) distributions that propagate uncertainty through the model in a backward direction. They are computed by a backward pass through the entire time series, analogous to a Kalman smoother. The backward message (Gaussian distribution) to  $S_0$  is computed by propagating Gaussian distributions for the inputs ( $P$ ,  $E$ , and  $Q$ ) and for  $S$  through the water balance back to  $S_0$ :

$$\text{backward message to } S_0 = \mathcal{N}(S_0 | m_S - m_P + m_E + m_Q, v_S + v_P + v_E + v_Q) \quad (\text{B5})$$

where the mean  $m_S$  and variance  $v_S$  of the backward message from  $S$  are obtained by multiplying the backward message to  $S$  (computed in previous step of backward pass) with the Gaussian likelihood of a GRACE observation, if any, using the same Gaussian multiplication formula given above. The posterior for each  $S$  (or  $S_0$ ) is obtained by multiplying the forward and backward message it receives as well as a GRACE likelihood message, if any.

Backward messages to the inputs are computed in a similar way:

$$\text{backward message to } P = \mathcal{N}(P | m_S - m_{S_0} + m_E + m_Q, v_{S_0} + v_S + v_E + v_Q) \quad (\text{B6})$$

$$\text{backward message to } E = \mathcal{N}(E | m_{S_0} - m_S + m_P - m_Q, v_{S_0} + v_S + v_P + v_Q) \quad (\text{B7})$$

$$\text{backward message to } Q = \mathcal{N}(Q | m_{S_0} - m_S + m_P - m_E, v_{S_0} + v_S + v_P + v_E) \quad (\text{B8})$$

These backward messages correspond to what Pan and Wood (2006) call a “constrained Kalman filter.” The product of these backward messages and the corresponding priors gives the posterior for each input. However, since  $P$ ,  $E$ , and  $Q$  are constrained to be positive, the actual posteriors are truncated Gaussians. Moments of each truncated posterior are given by

$$\mathbb{E}[x^n] = Z^{-1} \int_0^\infty x^n p(x)b(x)dx \quad (\text{B9})$$

where  $x$  is  $P$ ,  $E$ , or  $Q$ ,  $n = 1, 2$ ,  $p(x)$  is the unconstrained Gaussian prior of  $x$ ,  $b(x)$  is the backward message to  $x$  (Equations B6–B8), and  $Z = \int_0^\infty p(x)b(x)dx$ . The posterior is then approximated by a Gaussian with the mean equal to  $\mathbb{E}[x]$  and the variance equal to  $\mathbb{E}[x^2] - \mathbb{E}[x]^2$ . Finally, using a Gaussian division formula analogous to the Gaussian multiplication formula given earlier, the input messages used in Equations B1 and B5 are computed by dividing the approximate Gaussian posterior by the corresponding backward message  $b(x)$ . This creates a mutual dependence that is solved by iteration: repeat forward and backward passes over the entire time series until the approximate posteriors do not change anymore.

## Data Availability Statement

Data and code used in this study are available at <http://doi.org/10.5281/zenodo.4116451>.

## Acknowledgments

This work was supported by the Dutch Research Council (NWO) Visitor Travel Grant no. 040.11.731.

## References

- Abrishamchi, A., & Tajrishy, M. (2005). Interbasin water transfers in Iran. In *Water conservation, reuse, and recycling: Proceedings of an Iranian-American workshop*. National Academies Press.
- Aires, F. (2014). Combining datasets of satellite-retrieved products. Part I: Methodology and water budget closure. *Journal of Hydrometeorology*, 15(4), 1677–1691. <https://doi.org/10.1175/jhm-d-13-0148.1>
- Alemohammad, S., McColl, K., Konings, A., Entekhabi, D., & Stoffelen, A. (2015). Characterization of precipitation product errors across the US using multiplicative triple collocation. *Hydrology and Earth System Sciences*, 12(2). <https://doi.org/10.5194/hessd-12-2527-2015>
- Allam, M. M., Jain Figueroa, A., McLaughlin, D. B., & Eltahir, E. A. B. (2016). Estimation of evaporation over the upper Blue Nile basin by combining observations from satellites and river flow gauges. *Water Resources Research*, 52(2), 644–659. <https://doi.org/10.1002/2015wr017251>
- Bai, P., Liu, X., & Liu, C. (2018). Improving hydrological simulations by incorporating GRACE data for model calibration. *Journal of Hydrology*, 557, 291–304. <https://doi.org/10.1016/j.jhydrol.2017.12.025>
- Beck, H. E., Vergopolan, N., Pan, M., Levizzani, V., Van Dijk, A. I. J. M., Weedon, G. P., et al. (2017). Global-scale evaluation of 22 precipitation datasets using gauge observations and hydrological modeling. *Hydrology and Earth System Sciences*, 21(12), 6201–6217. <https://doi.org/10.5194/hess-21-6201-2017>
- Biancamaria, S., Mballo, M., Le Moigne, P., Sánchez Pérez, J. M., Espitalier-Noël, G., Grusson, Y., et al. (2019). Total water storage variability from GRACE mission and hydrological models for a 50,000 km<sup>2</sup> temperate watershed: The Garonne River basin (France). *Journal of Hydrology: Regional Studies*, 24, 100609. <https://doi.org/10.1016/j.ejrh.2019.100609>
- Chen, J., Wilson, C., Tapley, B., Save, H., & Cretaux, J.-F. (2017). Long-term and seasonal Caspian Sea level change from satellite gravity and altimeter measurements. *Journal of Geophysical Research: Solid Earth*, 122(3), 2274–2290. <https://doi.org/10.1002/2016JB013595>
- Chen, M., Senay, G. B., Singh, R. K., & Verdin, J. P. (2016). Uncertainty analysis of the Operational Simplified Surface Energy Balance (SSEBop) model at multiple flux tower sites. *Journal of Hydrology*, 536, 384–399. <https://doi.org/10.1016/j.jhydrol.2016.02.026>
- Döll, P., Fritsche, M., Eicker, A., & Müller Schmied, H. (2014). Seasonal water storage variations as impacted by water abstractions: Comparing the output of a global hydrological model with GRACE and GPS observations. *Surveys in Geophysics*, 35(6), 1311–1331. <https://doi.org/10.1007/s10712-014-9282-2>
- Forootan, E., Rietbroek, R., Kusche, J., Sharifi, M. A., Awange, J. L., Schmidt, M., et al. (2014). Separation of large scale water storage patterns over Iran using GRACE, altimetry and hydrological data. *Remote Sensing of Environment*, 140, 580–595. <https://doi.org/10.1016/j.rse.2013.09.025>
- Funk, C., Peterson, P., Landsfeld, M., Pedreros, D., Verdin, J., Rowland, J., et al. (2014). *A quasi-global precipitation time series for drought monitoring*. U.S. Geological Survey Data Series 832. US Geological Survey. Retrieved from <https://data.chc.ucs.edu/products/CHIRPS-2.0>
- Hobeichi, S., Abramowitz, G., Contractor, S., & Evans, J. (2020). Evaluating precipitation datasets using surface water and energy budget closure. *Journal of Hydrometeorology*, 21(5), 989–1009. <https://doi.org/10.1175/jhm-d-19-0255.1>
- Hobeichi, S., Abramowitz, G., Evans, J., & Ukkola, A. (2018). Derived optimal linear combination evapotranspiration (DOLCE): A global gridded synthesis ET estimate. *Hydrology and Earth System Sciences*, 22(2), 1317–1336. <https://doi.org/10.5194/hess-22-1317-2018>
- Horner, I., Renard, B., Le Coz, J., Branger, F., McMillan, H. K., & Pierrefeu, G. (2018). Impact of stage measurement errors on streamflow uncertainty. *Water Resources Research*, 54(3), 1952–1976. <https://doi.org/10.1002/2017wr022039>
- Huffman, G. J. (1997). Estimates of root-mean-square random error for finite samples of estimated precipitation. *Journal of Applied Meteorology*, 36(9), 1191–1201. [https://doi.org/10.1175/1520-0450\(1997\)036<1191:eormsr>2.0.co;2](https://doi.org/10.1175/1520-0450(1997)036<1191:eormsr>2.0.co;2)
- Huffman, G. J., Stocker, E., Bolvin, D., Nelkin, E., & Tan, J. (2019). *GPM IMERG Final Precipitation L3 1 month 0.1 degree × 0.1 degree V06*. Goddard Earth Sciences Data and Information Services Center (GES DISC). Retrieved from <https://gpm.nasa.gov/data/directory/IWRMC> (2020). *Iran Water Resources Management Company*. Retrieved from <http://wrs.wrm.ir/amar/login.asp>
- Jiang, L., Wu, H., Tao, J., Kimball, J. S., Alfieri, L., & Chen, X. (2020). Satellite-based evapotranspiration in hydrological model calibration. *Remote Sensing*, 12(3), 428. <https://doi.org/10.3390/rs12030428>
- Khaki, M., Forootan, E., Kuhn, M., Awange, J., van Dijk, A. I. J. M., Schumacher, M., & Sharifi, M. A. (2018). Determining water storage depletion within Iran by assimilating GRACE data into the W3RA hydrological model. *Advances in Water Resources*, 114, 1–18. <https://doi.org/10.1016/j.advwatres.2018.02.008>

- Khan, M. S., Liaqat, U. W., Baik, J., & Choi, M. (2018). Stand-alone uncertainty characterization of GLEAM, GLDAS and MOD16 evapotranspiration products using an extended triple collocation approach. *Agricultural and Forest Meteorology*, 252, 256–268. <https://doi.org/10.1016/j.agrformet.2018.01.022>
- Kiang, J. E., Gazoorian, C., McMillan, H., Coxon, G., Le Coz, J., Westerberg, I. K., et al. (2018). A comparison of methods for streamflow uncertainty estimation. *Water Resources Research*, 54(10), 7149–7176. <https://doi.org/10.1029/2018wr022708>
- Liu, W., Wang, L., Zhou, J., Li, Y., Sun, F., Fu, G., et al. (2016). A worldwide evaluation of basin-scale evapotranspiration estimates against the water balance method. *Journal of Hydrology*, 538, 82–95. <https://doi.org/10.1016/j.jhydrol.2016.04.006>
- Long, D., Longuevergne, L., & Scanlon, B. R. (2014). Uncertainty in evapotranspiration from land surface modeling, remote sensing, and GRACE satellites. *Water Resources Research*, 50(2), 1131–1151. <https://doi.org/10.1002/2013wr014581>
- Lopez, P. L., Sutanudjaja, E. H., Schellekens, J., Sterk, G., & Bierkens, M. F. (2017). Calibration of a large-scale hydrological model using satellite-based soil moisture and evapotranspiration products. *Hydrology and Earth System Sciences*, 21(6), 3125–3144.
- Maghsood, F. F., Hashemi, H., Hosseini, S. H., & Berndtsson, R. (2020). Ground validation of GPM IMERG precipitation products over Iran. *Remote Sensing*, 12(1), 48.
- Martens, B., Miralles, D. G., Lievens, H., Van Der Schalie, R., De Jeu, R. A. M., Fernández-Prieto, D., et al. (2017). GLEAM v3: Satellite-based land evaporation and root-zone soil moisture. *Geoscientific Model Development*, 10(5), 1903–1925. <https://doi.org/10.5194/gmd-10-1903-2017>
- Massari, C., Crow, W., & Brocca, L. (2017). An assessment of the performance of global rainfall estimates without ground-based observations. *Hydrology and Earth System Sciences*, 21(9), 4347–4361. <https://doi.org/10.5194/hess-21-4347-2017>
- Massari, C., & Maggioni, V. (2020). Error and uncertainty characterization. In *Satellite precipitation measurement* (pp. 515–532). Springer
- Minka, T. (2001). *A family of algorithms for approximate Bayesian inference* (Unpublished doctoral dissertation). Massachusetts Institute of Technology.
- Minka, T., Winn, J., Guiver, J., Zaykov, Y., Fabian, D., & Bronskill, J. (2018). *Infer.NET 0.3*. Microsoft Research Cambridge. Retrieved from <http://dotnet.github.io/infer>
- Moreira, A. A., Ruhoff, A. L., Roberti, D. R., de Arruda Souza, V., da Rocha, H. R., & de Paiva, R. C. D. (2019). Assessment of terrestrial water balance using remote sensing data in South America. *Journal of Hydrology*, 575, 131–147. <https://doi.org/10.1016/j.jhydrol.2019.05.021>
- Mueller, B., Seneviratne, S. I., Jimenez, C., Corti, T., Hirschi, M., Balsamo, G., et al. (2011). Evaluation of global observations-based evapotranspiration datasets and IPCC AR4 simulations. *Geophysical Research Letters*, 38(6). <https://doi.org/10.1029/2010gl046230>
- Munier, S., Aires, F., Schlaffer, S., Prigent, C., Papa, F., Maisongrande, P., & Pan, M. (2014). Combining data sets of satellite-retrieved products for basin-scale water balance study: 2. Evaluation on the Mississippi basin and closure correction model. *Journal of Geophysical Research: Atmospheres*, 119(21), 12–100. <https://doi.org/10.1002/2014jd021953>
- Oduanya, A. E., Mehdi, B., Schürz, C., Oke, A. O., Awokola, O. S., Awomeso, J. A., et al. (2019). Multi-site calibration and validation of SWAT with satellite-based evapotranspiration in a data-sparse catchment in southwestern Nigeria. *Hydrology and Earth System Sciences*, 23(2), 1113–1144. <https://doi.org/10.5194/hess-23-1113-2019>
- Pan, M., Sahoo, A. K., Troy, T. J., Vinukollu, R. K., Sheffield, J., & Wood, E. F. (2012). Multisource estimation of long-term terrestrial water budget for major global river basins. *Journal of Climate*, 25(9), 3191–3206. <https://doi.org/10.1175/jcli-d-11-00300.1>
- Pan, M., & Wood, E. F. (2006). Data assimilation for estimating the terrestrial water budget using a constrained ensemble Kalman filter. *Journal of Hydrometeorology*, 7(3), 534–547. <https://doi.org/10.1175/jhm495.1>
- Pellet, V., Aires, F., Munier, S., Fernández Prieto, D., Jordá, G., Dorigo, W. A., et al. (2019). Integrating multiple satellite observations into a coherent dataset to monitor the full water cycle - Application to the Mediterranean region. *Hydrology and Earth System Sciences*, 23(1), 465–491. <https://doi.org/10.5194/hess-23-465-2019>
- Rientjes, T. H. M., Muthuwatta, L. P., Bos, M. G., Booi, M. J., & Bhatti, H. A. (2013). Multi-variable calibration of a semi-distributed hydrological model using streamflow data and satellite-based evapotranspiration. *Journal of Hydrology*, 505, 276–290. <https://doi.org/10.1016/j.jhydrol.2013.10.006>
- Rodell, M., Beaudoing, H. K., L'Ecuyer, T. S., Olson, W. S., Famiglietti, J. S., Houser, P. R., et al. (2015). The observed state of the water cycle in the early twenty-first century. *Journal of Climate*, 28(21), 8289–8318. <https://doi.org/10.1175/jcli-d-14-00555.1>
- Sahoo, A. K., Pan, M., Troy, T. J., Vinukollu, R. K., Sheffield, J., & Wood, E. F. (2011). Reconciling the global terrestrial water budget using satellite remote sensing. *Remote Sensing of Environment*, 115(8), 1850–1865. <https://doi.org/10.1016/j.rse.2011.03.009>
- Save, H. (2020). *CSR GRACE and GRACE-FO RL06 mascon solutions v02*. <https://doi.org/10.15781/cgq9-nh24>
- Scanlon, B. R., Zhang, Z., Rateb, A., Sun, A., Wiese, D., Save, H., et al. (2019). Tracking seasonal fluctuations in land water storage using global models and GRACE satellites. *Geophysical Research Letters*, 46(10), 5254–5264. <https://doi.org/10.1029/2018gl081836>
- Scanlon, B. R., Zhang, Z., Save, H., Sun, A. Y., Müller Schmied, H., Van Beek, L. P. H., et al. (2018). Global models underestimate large decadal declining and rising water storage trends relative to GRACE satellite data. *Proceedings of the National Academy of Sciences*, 115(6), E1080–E1089. <https://doi.org/10.1073/pnas.1704665115>
- Schmidt, R., Petrovic, S., Güntner, A., Barthelmes, F., Wunsch, J., & Kusche, J. (2008). Periodic components of water storage changes from grace and global hydrology models. *Journal of Geophysical Research: Solid Earth*, 113(B8). <https://doi.org/10.1029/2007jb005363>
- Senay, G. B., Kagone, S., & Velpuri, N. M. (2020). Operational global actual evapotranspiration: Development, evaluation, and dissemination. *Sensors*, 20(7), 1915. <https://doi.org/10.3390/s20071915>
- Simons, G., Bastiaanssen, W., Ngó, L., Hain, C., Anderson, M., & Senay, G. (2016). Integrating global satellite-derived data products as a pre-analysis for hydrological modelling studies: A case study for the Red River basin. *Remote Sensing*, 8(4), 279. <https://doi.org/10.3390/rs8040279>
- ter Braak, C. J. F., & Vrugt, J. A. (2008). Differential evolution Markov chain with snooker updater and fewer chains. *Statistics and Computing*, 18(4), 435–446. <https://doi.org/10.1007/s11222-008-9104-9>
- Tian, Y., & Peters-Lidard, C. D. (2010). A global map of uncertainties in satellite-based precipitation measurements. *Geophysical Research Letters*, 37(24). <https://doi.org/10.1029/2010gl046008>
- Wan, Z., Zhang, K., Xue, X., Hong, Z., Hong, Y., & Gourley, J. J. (2015). Water balance-based actual evapotranspiration reconstruction from ground and satellite observations over the conterminous United States. *Water Resources Research*, 51(8), 6485–6499. <https://doi.org/10.1002/2015wr017311>
- Wang, S., Huang, J., Yang, D., Pavlic, G., & Li, J. (2015). Long-term water budget imbalances and error sources for cold region drainage basins. *Hydrological Processes*, 29(9), 2125–2136. <https://doi.org/10.1002/hyp.10343>
- Weerasinghe, I., Griensven, A. v., Bastiaanssen, W., Mul, M., & Jia, L. (2019). Can we trust remote sensing ET products over Africa? *Hydrology and Earth System Sciences Discussions*, 24(3), 1565–1586. <https://doi.org/10.5194/hess-24-1565-2020>

- Wiese, D. N., Landerer, F. W., & Watkins, M. M. (2016). Quantifying and reducing leakage errors in the JPL RL05M GRACE mascon solution. *Water Resources Research*, 52(9), 7490–7502. <https://doi.org/10.1002/2016wr019344>
- Wiese, D. N., Yuan, D., Boening, C., Landerer, F., & Watkins, M. (2018). *JPL GRACE mascon ocean, ice, and hydrology equivalent water height, release 06, coastal resolution improvement (CRI) filtered version 1.0*. PO.DAAC. Retrieved from <https://grace.jpl.nasa.gov/data>
- Yang, X., Yong, B., Ren, L., Zhang, Y., & Long, D. (2017). Multi-scale validation of GLEAM evapotranspiration products over China via ChinaFLUX ET measurements. *International Journal of Remote Sensing*, 38(20), 5688–5709. <https://doi.org/10.1080/01431161.2017.1346400>
- Zhang, L., Dobslaw, H., Stacke, T., Güntner, A., Dill, R., & Thomas, M. (2017). Validation of terrestrial water storage variations as simulated by different global numerical models with GRACE satellite observations. *Hydrology and Earth System Sciences*, 21(2), 821–837. <https://doi.org/10.5194/hess-21-821-2017>
- Zhang, Y., Pan, M., Sheffield, J., Siemann, A. L., Fisher, C. K., Liang, M., et al. (2018). A Climate Data Record (CDR) for the global terrestrial water budget: 1984–2010. *Hydrology and Earth System Sciences*, 22(1), 241–263. <https://doi.org/10.5194/hess-22-241-2018>
- Zhang, Y., Pan, M., & Wood, E. F. (2016). On creating global gridded terrestrial water budget estimates from satellite remote sensing. *Surveys in Geophysics*, 37(2), 249–268. <https://doi.org/10.1007/s10712-015-9354-y>